JCB Journal of Cell Biology

ARTICLE

CLPTM1L is a GPI-anchoring pathway component targeted by HCMV

Inbal Kol[1], Ahmed Rishiq[1], Mevaseret Cohen[1], Shira Kahlon[1], Ophir Pick[1], Liat Dassa[1], Natan Stein[1], Yotam Bar-On[2], Dana G. Wolf[1,3], Einat Seidel[1]*, and Ofer Mandelboim[1]*

The GPI-anchoring pathway plays important roles in normal development and immune modulation. MHC Class I Polypeptide-related Sequence A (MICA) is a stress-induced ligand, downregulated by human cytomegalovirus (HCMV) to escape immune recognition. Its most prevalent allele, MICA*008, is GPI-anchored via an uncharacterized pathway. Here, we identify cleft lip and palate transmembrane protein 1-like protein (CLPTM1L) as a GPI-anchoring pathway component and show that during infection, the HCMV protein US9 downregulates MICA*008 via CLPTM1L. We show that the expression of some GPI-anchored proteins (CD109, CD59, and MELTF)—but not others (ULBP2, ULBP3)—is CLPTM1L-dependent, and further show that like MICA*008, MELTF is downregulated by US9 via CLPTM1L during infection. Mechanistically, we suggest that CLPTM1L's function depends on its interaction with a free form of PIG-T, normally a part of the GPI transamidase complex. We suggest that US9 inhibits this interaction and thereby downregulates the expression of CLPTM1L-dependent proteins. Altogether, we report on a new GPI-anchoring pathway component that is targeted by HCMV.

Introduction

The effects of viruses on a broad range of cellular activities have recently gained increasing interest. One of the affected pathways is that of glycosylphosphatidylinositol (GPI) anchoring. This includes biosynthesis of the GPI moiety, its attachment to precursor proteins, and remodeling and transport of nascent GPI-anchored proteins to the cell surface. Evidence that constituents of this pathway and the resultant GPI-anchored proteins play roles in immune modulation and in normal development has accumulated in recent years (Hussein et al., 2020; Manea, 2018; Gennarini et al., 2017; Kinoshita, 2020).

MHC Class I Polypeptide-related Sequence A (MICA) is a member of a family of eight stress-induced ligands, all recognized by the natural killer (NK) cell activating receptor Natural Killer Group 2D (NKG2D). Upon cellular stress, such as viral infection, MICA and other members of this family of ligands are upregulated, leading to killing of potentially hazardous cells by NK cells and T cells (Schmiedel and Mandelboim, 2018; Raulet et al., 2013). To evade NKG2D-mediated recognition, many viruses have developed mechanisms to downregulate these ligands (Diab et al., 2020; Bauman et al., 2016; Nachmani et al., 2009). One such virus is the human cytomegalovirus (HCMV), which possesses a large and complex double-stranded DNA genome, much of it dedicated to immune-evasion strategies (Jackson et al., 2011; Amsler et al., 2013; Wilkinson et al., 2008).

MICA is highly polymorphic, having more than 250 known alleles (Robinson et al., 2020). Its most prevalent allele, MICA*008, accounts for up to 50% of all MICA alleles in diverse human populations (Ashiru et al., 2013; Klussmeier et al., 2020; Risti and Bicalho, 2017). While most alleles contain transmembrane (TM) domains, MICA*008 is first synthesized as a truncated soluble protein due to a frameshift mutation in the TM domain. It is then "rescued" and expressed on the cell surface through attachment to a GPI anchor, resulting in different biological properties when compared to full-length MICA alleles, including preferential localization to detergent-resistant membranes, shedding by exosomes, and apical sorting (Suemizu et al., 2002; Ashiru et al., 2010; Ashiru et al., 2013).

Proteins entering the ER lumen are destined to be GPI-anchored if they encode a GPI-attachment signal (GAS). Although poorly conserved in terms of its sequence, the GAS is composed of several known biophysical characteristics, namely, a GPI-attachment site (the ω-site), followed by a hydrophobic C-terminal domain (the pro-peptide), which is cleaved off upon GPI moiety attachment (Kinoshita, 2020; Gerber et al., 1992). Both cleavage and attachment processes are executed by the GPI

[1]The Concern Foundation Laboratories at the Lautenberg Center for Immunology and Cancer Research, Institute for Medical Research Israel Canada, Hadassah—Hebrew University Medical Center, Jerusalem, Israel; [2]Department of Immunology, Technion-Israel Institute of Technology, Haifa, Israel; [3]Clinical Virology Unit, Hadassah Hebrew University Medical Center, Jerusalem, Israel.

*E. Seidel and O. Mandelboim contributed equally to this paper. Correspondence to Ofer Mandelboim: oferm@ekmd.huji.ac.il; Inbal Kol: inbalhod@gmail.com.

transamidase complex (TAC), which consists of GPI anchor attachment 1 protein and phosphatidylinositol glycan classes -K (PIG-K), -U (PIG-U), -S (PIG-S), and -T (PIG-T; Kinoshita, 2020). The GPI moiety itself is synthesized in a stepwise process of 11 reactions, which is initiated on the cytoplasmic side of the ER, and ends in the ER lumen with a mature GPI precursor competent for attachment (Kinoshita, 2020).

The duration of the GPI-anchoring process, from protein synthesis to cell-surface expression of the mature form, ranges from 30 min to 2 h (Takida et al., 2008; Fernández-Messina et al., 2011; Fernández-Messina et al., 2012; Hein et al., 2009; Fernández-Messina et al., 2016), whereas for MICA*008 it takes an astonishing 19 h (Ashiru et al., 2013). Due to these unusually slow kinetics and the fact that most prediction tools are unable to identify a GAS in MICA*008, it was hypothesized that MICA*008 utilizes a non-standard GPI-anchoring pathway (Seidel et al., 2021a; Seidel et al., 2015; Ashiru et al., 2013).

Recently (Seidel et al., 2021a; Seidel et al., 2015), we showed that the HCMV protein US9 downregulates MICA*008 in two ways: (1) maturation arrest of MICA*008 prior to the GPI-anchoring step and (2) the induction of proteasomal degradation via the SEL1L-HRD1 ER-associated degradation (ERAD) complex. Mechanistically, we showed that these effects are mediated predominantly via the US9 signal peptide (9SP), which is cleaved unusually slowly. Retained 9SP arrests MICA*008 maturation, indirectly leading to its degradation via physiological ER quality control processes timed by the progressive trimming of N-glycosylation mannose residues on maturation-arrested MICA*008.

Importantly, 9SP alone was sufficient for induction of MICA*008 maturation arrest and degradation even when fused to different proteins (Seidel et al., 2021a). A secondary, less significant mechanism of US9 action is mediated via its Ig-like and TM domains, which directly bind MICA*008 and SEL1L, respectively, inducing mannose-trimming independent degradation of MICA*008. The 9SP-mediated maturation arrest, we theorized, occurs via inhibition of cellular components of a non-standard GPI-anchoring pathway, and without it, the truncated and frameshifted allele was recognized as misfolded and disposed of (Fig. 1 A). We further postulated that these cellular components would be membrane-bound, to explain how 9SP, itself a short TM peptide, could interact with them.

Here, we show that the cellular interaction partner which 9SP binds and acts upon is cleft lip and palate transmembrane protein 1-like protein/cisplatin resistance related protein 9 (CLPTM1L/CRR9), an ER-resident protein (James et al., 2012; Ni et al., 2012; James et al., 2014; Ni et al., 2016; Yamamoto et al., 2001), with no known function in protein maturation. We identified additional proteins whose expressions are dependent on CLPTM1L and identified mechanisms of CLPTM1L-mediated GPI-anchoring and how 9SP acts upon CLPTM1L to inhibit the GPI-anchoring of MICA*008 and other CLPTM1L-dependent proteins.

Results

9SP downregulates MICA*008 but does not co-precipitate with it

We have previously shown that deletion of 9SP did not affect US9's interaction with MICA*008, indicating there was no direct interaction between 9SP and MICA*008 (Seidel et al., 2021a). We therefore hypothesized that 9SP acts by inhibiting cellular components of MICA*008's non-standard GPI-anchoring pathway (Fig. 1 A). To test this hypothesis, we used previously described US9 mutants overexpressed in RKO cells (a poorly differentiated colon carcinoma cell line) expressing MICA*008 (named RKO*008; Seidel et al., 2015). RKO cells endogenously express minimal levels of the full-length MICA allele *007:01, and we therefore transduced them with MICA*008, fused to an N-terminal HA tag. The US9 constructs used, all containing a C-terminal HIS tag, were wild-type (wt) US9, wt US8 (an HCMV protein with limited homology to US9 which targets toll-like receptor pathways [Park et al., 2019]), US9 in which the SP was swapped to that of US8 (sw8SP), and a US8 mutant in which the signal peptide was swapped to 9SP (sw9SP; Fig. 1 B). We also used RKO*008 empty vector (EV) for control.

First, we checked surface MICA*008 levels in the RKO*008 EV, US9, sw8SP, US8, and sw9SP cells using flow cytometry (FCM). As previously described, US9 caused significant downregulation of MICA*008 as compared with the EV (Fig. 1 C). Sw8SP (containing US9's Ig-like and TM domains) was still able to induce MICA*008's downregulation, but to a lesser extent (Fig. 1 C), as expected. Similarly, sw9SP retained 9SP's function, while US8 had no effect on MICA*008 (Fig. 1 D).

We then performed a co-immunoprecipitation (Co-IP) assay using an α-HIS antibody (Ab) to examine whether the different mutants directly interact with MICA*008. Cell lysates before precipitation were used as input control. As we have previously reported (Seidel et al., 2021a), US9 migrated as two distinct protein bands, representing a larger, slowly cleaved SP^+ precursor form and a smaller SP^- processed form. This two-band appearance is lost in the sw8SP mutant and wt US8 construct in which the SP is rapidly processed. The sw9SP mutant migrates as a single band as well, slightly higher than the wt US8 construct, which is consistent with a constitutively retained SP (Fig. S1 A).

We have previously shown that in RKO cells, MICA*008 migrates in Western blot (WB) in two distinct bands: a larger ∼70-kD "smear," which corresponds to post-ER mature GPI^+ forms, and a smaller ∼60-kD band which corresponds to an ER-resident, immature, mostly GPI^- form (Seidel et al., 2021a; Seidel et al.,2015). These size differences are caused by glycosylation modifications acquired in the Golgi apparatus (Seidel et al., 2015). In this Co-IP assay, however, only the detergent-soluble fraction was extracted due to the lysis buffer used (NP40). For this reason, the only MICA*008 band that was observed was the smaller, ER-resident, mostly GPI^- form (Fig. 1 E). As expected, only US9 and sw8SP specifically precipitated with MICA*008 as they contain the Ig-like domain of US9, while US8 and sw9SP did not, despite sw9SP's significant effect on MICA*008 expression (Fig. 1 E and Fig. S1 A). These results verify that 9SP affects MICA*008 despite the lack of any direct interaction between the two.

CLPTM1L is a cellular factor specifically bound by 9SP

To identify the postulated cellular target of 9SP through which it affects MICA*008, we first looked for proteins that are bound by

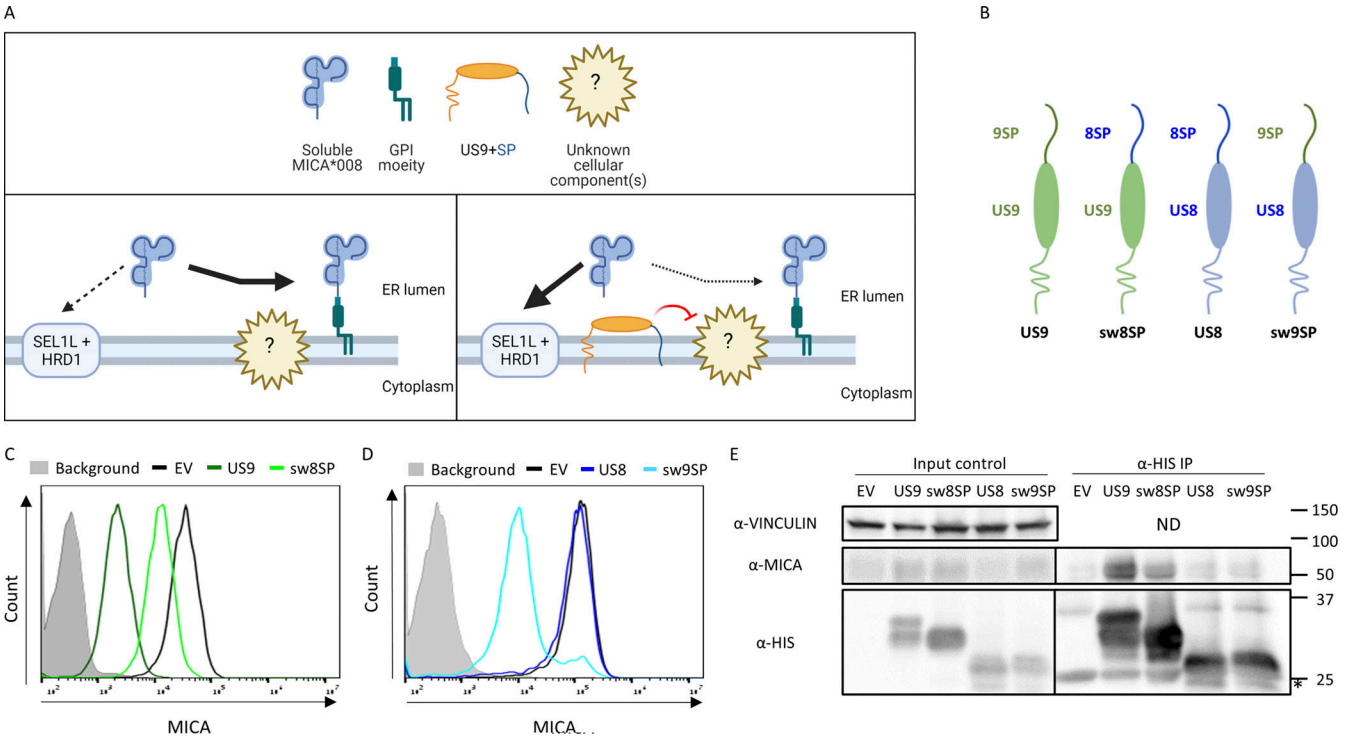

Figure 1. **9SP downregulates MICA*008 but does not co-precipitate with it. (A)** Model for 9SP's indirect effect on MICA*008: under normal conditions (left) soluble MICA*008 is "rescued" from the ERAD proteins SEL1L and HRD1 by unknown component(s) of the GPI-anchoring pathway, causing MICA*008 to be expressed as a GPI-anchored protein. In the presence of 9SP (right), the aforementioned GPI-anchoring pathway component(s) is inhibited (highlighted in red). Soluble MICA*008 in the ER is no longer GPI-anchored, and instead, it is degraded via the ERAD proteins SEL1L and HRD1. **(B)** US9 mutants used in this paper, all containing a C-terminal HIS tag. **(C)** RKO*008 cells co-expressing either an EV (black line), US9 (dark green line), or a US9 mutant in which the signal peptide was swapped with that of US8 (sw8SP, light green line) were stained with α-MICA Ab. Secondary Ab only was used as background (gray-filled histogram). **(D)** RKO*008 cells co-expressing either an EV (black line), US8 (dark blue line) or a US8 mutant in which the signal peptide was swapped with that of US9 (sw9SP, light blue line). Secondary Ab only was used as background (gray-filled histogram). **(E)** Co-IP performed in RKO*008 cells, co-expressing one of the following: EV, US9, sw8SP, US8, and sw9SP (all but the EV with a HIS-tag). Cell lysates before precipitation were used as input control. Precipitation was performed using α-HIS Ab; detection Abs are indicated next to each blot. ND, not detected. Asterisk indicates Ab light chain (~25 kD). Source data are available for this figure: SourceData F1.

9SP, speculating that these proteins could be a part of MICA*008's GPI-anchoring machinery. To this end, we performed a Co-IP assay using an α-HIS Ab, in US9 and sw9SP-expressing RKO MICA*008 cells. In addition, we repeated this screen in US9-expressing HeLa cells, which endogenously express MICA*008 (Zhang et al., 2001). RKO*008 EV, RKO*008 US8, and HeLa EV were used as negative controls. An additional isotype-matched control Ab was also used for US9-expressing cell types. Utilizing liquid chromatography with tandem mass spectrometry (LC-MS/MS), we identified proteins that precipitate with US9 in both cell types as well as with sw9SP. One of the top hits that consistently precipitated with 9SP-containing cells was a protein called CLPTM1L (Table S1 and Data S1). This ER-resident, membrane-spanning protein is best known for conferring resistance to apoptosis (James et al., 2012) and for its association with cisplatin resistance and cancer (Ni et al., 2012; Ni et al., 2016; Yamamoto et al., 2001; James et al., 2014). We therefore chose this protein for further analysis.

To corroborate this result, we repeated the Co-IP experiment in RKO*008 EV and US9 cells, this time specifically detecting CLPTM1L in WB. Cell lysates before precipitation were used as input control, showing that CLPTM1L can be detected in both cell types and the typical doublet appearance of US9 (Fig. 2 A). As expected, CLPTM1L could be detected in the eluate from US9 IP (Fig. 2 B). To verify that the US9 domain which binds CLPTM1L is indeed 9SP, we repeated this experiment in RKO*008 US8 and sw9SP cells. Cell lysates before precipitation were again used as input control, showing that CLPTM1L can be detected in both cell types (Fig. 2 C). Indeed, while CLPTM1L was not detected in US8 IP eluate, it was abundant in the sw9SP IP eluate (Fig. 2 D).

Since we only performed Co-IP of US9 with CLPTM1L in the context of US9 overexpression, we next examined whether levels of US9 in RKO*008 US9 cells are similar to the US9 levels observed during HCMV infection. To test this, we used MRC-5 fibroblasts that are permissive to HCMV infection and infected them with the HCMV wt AD169varL strain, which encodes the US9 protein. The infected cells were lysed at 24 h post infection (hpi), and US9 mRNA levels were evaluated using quantitative polymerase chain reaction (qPCR). We also evaluated levels of US9 mRNA in the RKO*008 US9 cells and compared the two (Fig. 2 E). The difference between the two cell types in US9 expression was not significant, suggesting similar levels.

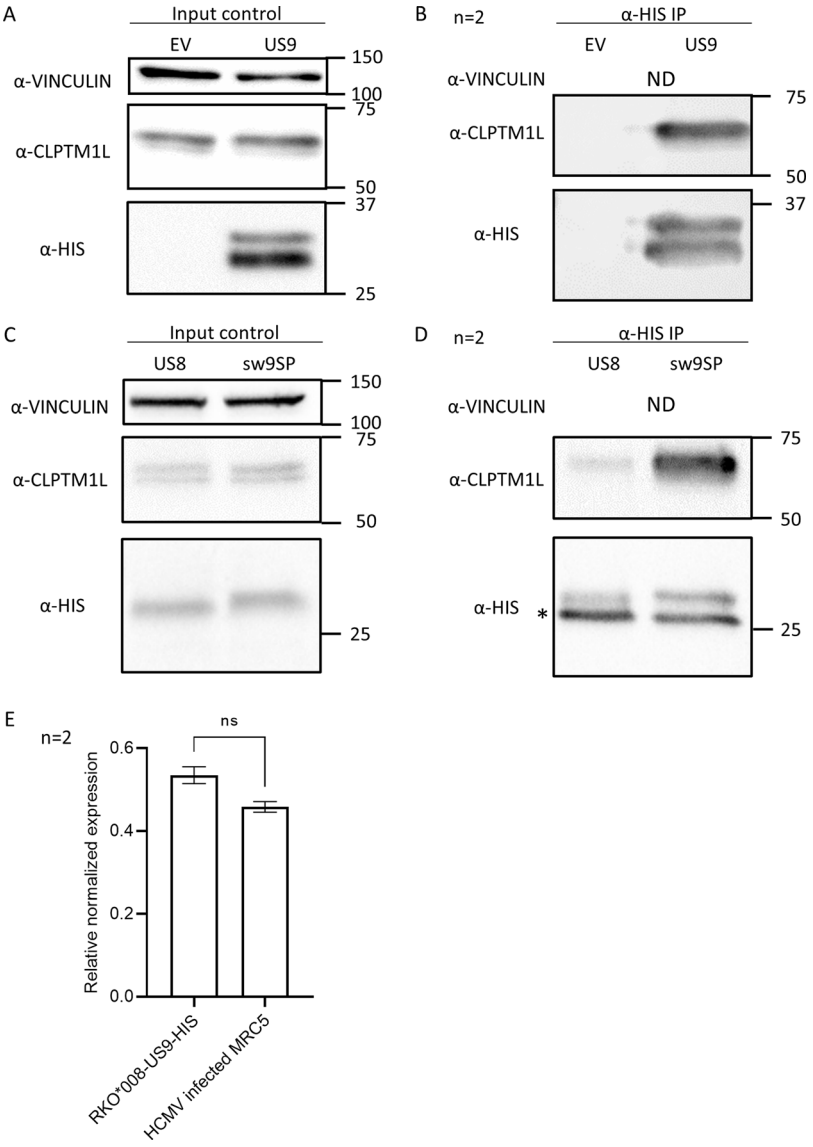

Figure 2. **CLPTM1L is a cellular factor specifically bound by 9SP. (A and B)** Co-IP performed in RKO*008 cells, co-expressing either EV or US9-HIS (US9). Detection Abs are indicated next to each blot. ND, not detected. **(A)** Cell lysates before precipitation were used as input control. **(B)** Precipitation Ab used was α-HIS. **(C and D)** Co-IP performed in RKO*008 cells, co-expressing either US8-HIS or sw9SP-HIS (US8 and sw9SP, respectively). Detection Abs are indicated next to each blot. ND, not detected. **(C)** Cell lysates before precipitation were used as input control. **(D)** Precipitation Ab used was α-HIS. Asterisk indicates Ab light chain (~25 kD). **(E)** Column bar graphs showing quantification of US9 mRNA in RKO*008 cells co-expressing US9-HIS (RKO*008-US9-HIS) and MRC-5 fibroblasts 24 hpi with HCMV AD169varL strain (HCMV infected MRC5). Figure shows mean (normalized to the endogenous reference genes hUBC and hHPRT) and SEM for two technical replicates. ns, non-significant; unpaired two-tailed *t* test. Source data are available for this figure: SourceData F2.

CLPTM1L is important for MICA*008 maturation and surface expression

Seeing as 9SP directly binds CLPTM1L, we were interested in the possible effects CLPTM1L has on MICA*008. To examine this, we knocked out CLPTM1L using CRISPR/cas9 single guide RNA (sgRNA) in RKO*008 cells (Fig. 3 A). Using FCM, we evaluated MICA*008 surface expression levels in parental and knock-out (KO) cells and observed a 17-fold downregulation in the KO cells (Fig. 3 B, quantified in Fig. S1 B), indicating CLPTM1L is required for proper MICA*008 expression.

We verified these results by generating CLPTM1L KO in 293T cells which endogenously express MICA*008 (McSharry et al., 2008; Fig. S1 C). We then used FCM to assess MICA*008 surface expression in 293T cells and observed a similarly robust downregulation of 14-fold in the KO cells (Fig. S1 D, quantified in Fig. S1 E). To confirm that CLPTM1L specifically caused the effect observed in the KO cells, we rescued the RKO*008 KO cells by reintroducing either an EV control (KO EV) or C-terminal FLAG-tagged CLPTM1L (Rescue C'FLAG) into the cells via lentiviral transduction (Fig. 3 C). By FCM, we determined that MICA*008's surface expression levels in the Rescue C'FLAG cells were fully restored compared with the level in the KO EV cells (Fig. 3 D).

Next, we wanted to determine whether CLPTM1L only affects surface expression of MICA*008 or also affects protein levels, and if so, at what stage in MICA*008's biogenesis the effect is seen. As mentioned, MICA*008 migrates in WB in two distinct bands, corresponding to its location in the cell and to its maturation level. We lysed RKO*008 parental, CLPTM1L KO, KO EV, and Rescue C'FLAG cells, and performed a WB with an α-MICA Ab to assess CLPTM1L's effect on the various MICA*008 forms. There was a reduction of MICA*008 protein levels in CLPTM1L KO cells, with a differential effect on the two MICA*008 forms; while the 60-kD ER-resident form was unaffected, the post-ER form was significantly reduced by approximately ninefold in the CLPTM1L KO cells (Fig. 3 E, MICA*008 post-ER form quantified in Fig. 3 F). This points to a process that occurs after MICA*008's synthesis but before its egress from the ER as a GPI-anchored protein. Notably, this MICA*008 downregulation pattern is

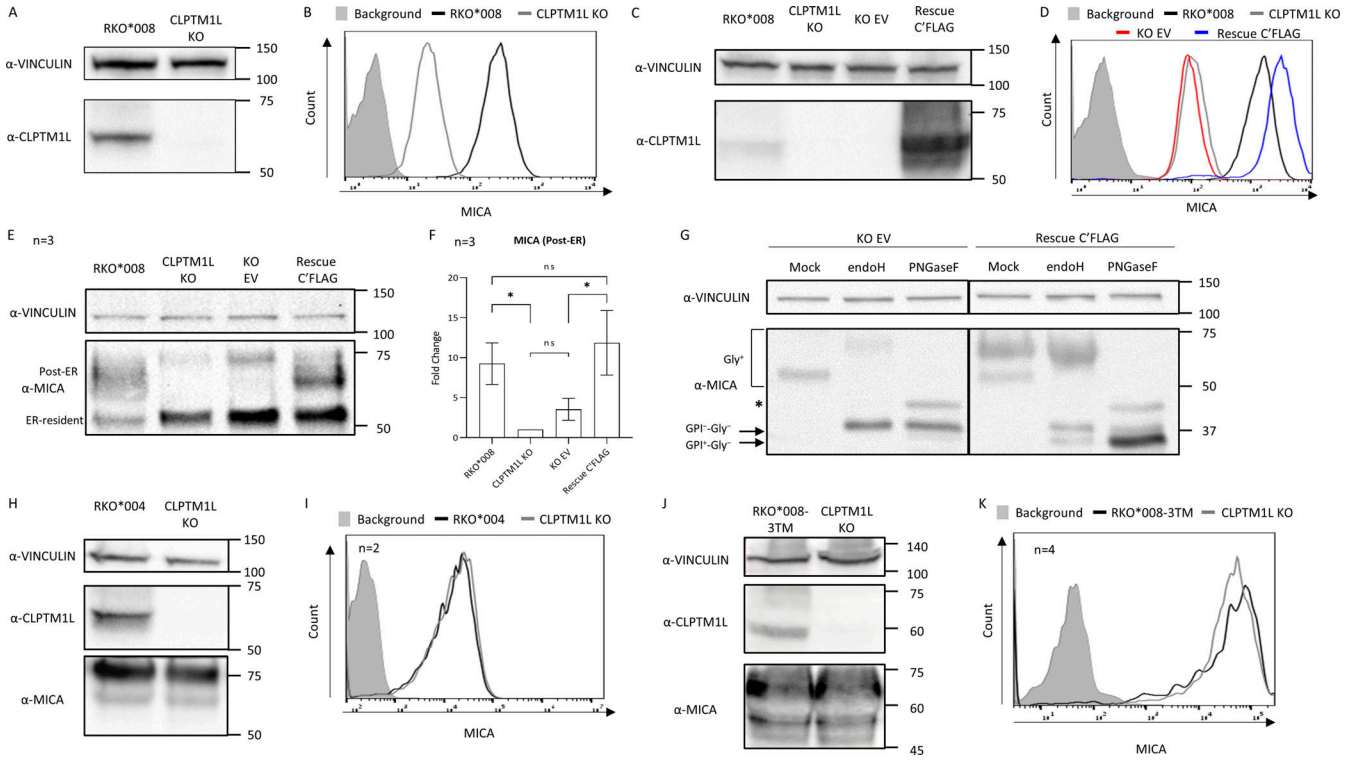

Figure 3. **CLPTM1L is important for MICA*008 maturation and surface expression. (A)** RKO*008 cells, either parental (RKO*008) or after CLPTM1L KO, were lysed and analyzed by WB. Detection Abs are indicated on the left. **(B)** Cells as in A were stained with α-MICA Ab and analyzed by FCM. RKO*008, black line, CLPTM1L KO, gray line. Background (secondary Ab only), gray-filled histogram. **(C)** RKO*008 and CLPTM1L KO cells, as well as CLPTM1L KO cells expressing an empty vector (KO EV) or a C'FLAG tagged CLPTM1L (Rescue C'FLAG), were lysed and analyzed by WB. Detection Abs are indicated on the left. **(D)** Cells as in C were stained with α-MICA Ab and analyzed by FCM. RKO*008, black line, CLPTM1L KO, gray line, KO EV, red line, Rescue C'FLAG, blue line. Background (secondary Ab only), gray-filled histogram. **(E)** Cells as in C were lysed and analyzed by WB. Detection Abs are indicated on the left. The ER-resident and post-ER forms of MICA*008 are indicated ("ER-resident" and "Post-ER," respectively). **(F)** Column bar graphs showing quantification of the mature MICA*008 band, calculated from three technical repeats of E, and after normalization to the loading control (VINCULIN). In each repetition, the band intensity is relative to that of CLPTM1L KO, which was defined as 1. A one-way ANOVA was performed with a significant effect at the $P < 0.01$ level for all conditions ($F[3, 8] = 12.13$, $P = 0.0024$). A post-hoc Sidak's multiple comparison test was used to compare RKO*008 to CLPTM1L KO and to Rescue C'FLAG, and KO EV to CLPTM1L KO and to Rescue C'FLAG. *, $P < 0.05$; ns, non-significant. Error bars represent SD. **(G)** KO EV and Rescue C'FLAG cell lysates were mock-treated or digested with either Endo H or PNGase F and analyzed by WB. Detection Abs are indicated next to each blot. The glycosylated forms range in size between 50 and 75 kD and are marked on the left ("Gly⁺"). The two deglycosylated forms of MICA, GPI-anchored ("GPI⁺-Gly⁻") and non-GPI-anchored ("GPI⁻-Gly⁻"), are marked with an arrow. The mature GPI⁺-Gly⁻ form runs faster due to the added negative charge of the GPI anchor. Asterisk indicates the endogenous MICA*007:001 form, found in low amounts on RKO cells (~45 kD). **(H)** RKO*004 cells, either parental or CLPTM1L KO, were lysed and analyzed by WB. Detection Abs are indicated next to each blot. **(I)** Cells as in H were stained with α-MICA Ab and analyzed by FCM. RKO*004, black line, CLPTM1L KO, gray line. Background (secondary Ab only), gray-filled histogram. **(J)** RKO cells which express the MICA*008-ULBP3TM chimera, either parental (RKO*008-3TM) or CLPTM1L KO, were lysed and analyzed by WB. Detection Abs are indicated next to each blot. **(K)** Cells as in J were stained with α-MICA Ab and analyzed by FCM. RKO*008-3TM, black line, CLPTM1L KO, gray line. Background (secondary Ab only), gray-filled histogram. Source data are available for this figure: SourceData F3.

identical to the pattern observed with US9 overexpression (Seidel et al., 2021a; Seidel et al., 2015). Similarly, we observed a restoration of the post-ER form and MICA*008 protein levels in the Rescue C'FLAG as compared with the KO EV cells (Fig. 3, E and F). We verified these results by repeating this assay in 293T parental and CLPTM1L KO cells (Fig. S1 F), again observing a specific reduction of the post-ER MICA*008 form in the CLPTM1L KO cells (shown by an arrow).

To verify the MICA*008 forms observed in the WB indeed correspond with those previously reported (Seidel et al., 2021a; Seidel et al., 2015), we digested cell lysates of KO EV and Rescue C'FLAG cells with Endoglycosidase H (Endo H) and Peptide:N-glycosidase F (PNGase F). These enzymes remove N-linked glycosylations, with Endo H acting only on unmodified core glycosylations, enabling detection of glycoproteins that have yet to pass through the Golgi apparatus. As a control, we used mock-treated cell lysates. It was previously reported that the GPI⁺ form runs at 34 kD upon deglycosylation and is mostly Endo H resistant as it has exited the ER (Ashiru et al., 2013; Seidel et al., 2015). The GPI⁻ form runs at 37 kD upon deglycosylation and is Endo H sensitive (Ashiru et al., 2013; Seidel et al., 2015). Indeed, digestion with PNGase F revealed that the ~70-kD smear (which is absent in the KO EV cells and reappears in the rescued cells) corresponds to the post-ER mature GPI⁺ form of MICA*008, and the 60-kD form is the Endo H–sensitive, ER-resident form of MICA*008 (Fig. 3 G). Notably, in the Rescue C'FLAG cells, some of the Endo H–sensitive MICA*008 was GPI-anchored, while no such bands could be detected in the KO cells, confirming the loss of the GPI-anchored form in the absence of CLPTM1L.

Since CLPTM1L is required for efficient MICA*008 GPI-anchoring, we wondered whether full-length MICA alleles, which are TM proteins, would be unaffected by CLPTM1L KO similarly to their resistance to US9. To test this hypothesis, we used the previously established RKO MICA*004 cell line (Seidel et al., 2015; RKO*004), which exogenously expresses the full-length MICA*004 allele fused to an N-terminal HA tag. We knocked out CLPTM1L in these cells (Fig. 3 H) and then used both WB (Fig. 3 H) and FCM (Fig. 3 I) to assess MICA*004 levels in these cells. As expected, MICA*004 levels remained unaffected in the KO cells.

We have previously shown that mutating MICA*008 to contain a canonical GAS sequence (derived from UL16-binding protein 3, ULBP3) instead of its TM domain makes it US9-resistant (Seidel et al., 2015). We were curious to see if CLPTM1L KO would be comparable with US9 overexpression in terms of its lack of effect on this mutant. To check this, we generated CLPTM1L KO in RKO cells expressing this mutant (RKO*008-3TM, Fig. 3 J). We then used both WB (Fig. 3 J) and FCM (Fig. 3 K, quantified in Fig. S1 G) to assess MICA*008-3TM levels in these cells and observed no significant difference.

In summary, these results indicate that CLPTM1L is a necessary component of MICA*008's GPI-anchoring pathway and that CLPTM1L KO phenotypically resembles US9 overexpression.

MICA*008 is downregulated by US9 via CLPTM1L during HCMV infection

Next, we wanted to determine the importance of CLPTM1L during HCMV infection. For this, we generated CLPTM1L KO in MRC-5 fibroblasts, which are homozygous for MICA*008 (Seidel et al., 2021a; Fig. 4 A). We then infected parental and CLPTM1L KO MRC-5 cells with two HCMV strains: the wt AD169varL strain ("WT") or its previously generated US9 deletion mutant ("ΔUS9"; Seidel et al., 2015). The infected cells were harvested at 72 hpi (at which point US9 reaches peak effect; Seidel et al., 2015; Seidel et al., 2021a) and the surface expression level of MICA*008 was evaluated using FCM. We used uninfected cells of each cell type for control ("N.I," not infected).

In parental cells, as expected, MICA*008 was significantly downregulated following infection with the WT virus and to a lesser extent in ΔUS9-infected cells (Fig. 4 B, left panel, quantified in Fig. 4 C). The non-significant downregulation in MICA*008 still observed in ΔUS9-infected cells is in accordance with previously published results, which suggested that during HCMV infection, the effect of US9 deletion is only partial due to additional viral factors that target MICA*008 (Seidel et al., 2015; Seidel et al., 2021b). As expected, MICA*008 was significantly downregulated in the CLPTM1L KO cells and there was no significant difference in MICA*008 levels between WT- and ΔUS9-infected cells (Fig. 4 B, right panel, quantified in Fig. 4 C). This confirms that CLPTM1L is indeed a cellular mediator of US9's effect over MICA*008.

CLPTM1L plays a role in the expression of additional GPI-anchored proteins

Having established CLPTM1L's role in MICA*008 biogenesis, we wanted to assess whether CLPTM1L's function is unique to MICA*008 or rather shared with other GPI-anchored proteins.

We decided to search for additional GPI-anchored targets using phosphoinositide phospholipase C (PI-PLC), an enzyme that cleaves GPI-anchored proteins from their anchor, releasing them into the medium. We treated either 293T parental or CLPTM1L KO cells with PI-PLC (parental-PI-PLC or KO-PI-PLC samples, respectively) and analyzed the supernatants using LC-MS/MS (Fig. 5 A and Data S2). As a negative control, cells were mock-treated (MT) under the same conditions but with no enzyme (parental-MT and KO-MT samples, respectively). We searched the results for proteins that were specifically enriched in the parental-PI-PLC sample as compared with both the KO-PI-PLC sample and the parental-MT samples, suggesting that their expression level or susceptibility to PI-PLC treatment was CLPTM1L-dependent. As a positive control, we verified (using WB) that cleaved MICA*008 could be detected only in the parental-PI-PLC supernatant sample (Fig. 5 B).

After selection criteria were applied, the six proteins most highly enriched in the parental-PI-PLC sample were CD109, melanotransferrin (MELTF), Glypican 4, Reticulon-4 receptor-like 2, Glypican 6 (GPC6), and CD59. Notably, all six proteins are known to be GPI-anchored and contain a canonical GAS. This was interesting, as we speculated that other CLPTM1L-dependent proteins may not contain a classic GAS, similar to MICA*008.

Since we were specifically interested in CLPTM1L-dependent proteins that might also be HCMV targets, we searched the literature for the levels of these six proteins throughout the course of HCMV infection. Indeed, in previously published surface and total cell proteomics data (Weekes et al., 2014), the surface levels of four out of the six proteins (CD109, MELTF, GPC6, and CD59) were shown to decrease at different time points during infection of human foreskin fibroblasts (Fig. S2). We therefore chose these four proteins for further assessment by FCM, comparing their surface expression in parental and CLPTM1L KO RKO*008 and 293T cells using specific Abs. CD109 and CD59 were mildly downregulated by 1.2- to 1.6-fold in the KO cells in both RKO*008 and 293T cells (Fig. 5, C and D, respectively, quantified in Fig. S3, A and B, respectively). MELTF, on the other hand, was more efficiently downregulated in KO RKO*008 (Fig. 5 C, quantified in Fig. S3 A) and 293T cells (Fig. 5 D, quantified in Fig. S3 B). In contrast, GPC6 showed minimal baseline expression, and no effect of KO was observed (Fig. 5, C and D, not quantified).

Since the three new CLPTM1L-dependent proteins we discovered all contain a canonical GAS, we next wondered if all GPI-anchored proteins are CLPTM1L-dependant to some extent. In particular, we were interested to examine the role of CLPTM1L in the production of other GPI-anchored NKG2D ligands, such as ULBP2 and ULBP3. The expression of ULBP3 was already examined indirectly with the staining of RKO*008-3TM cells (Fig. 3, J and K; and Fig. S1 G), and it is unaffected by CLPTM1L. Nonetheless, we stained for both proteins in parental and CLPTM1L KO RKO*008 and 293T cells. The expression level of both proteins was not affected by CLPTM1L KO, both in RKO*008 and 293T cells (Fig. 5, C and D, respectively, quantified in Fig. S3, A and B, respectively).

In conclusion, we found that three additional GPI-anchored proteins (CD109, CD59, and MELTF) also depend on CLPTM1L

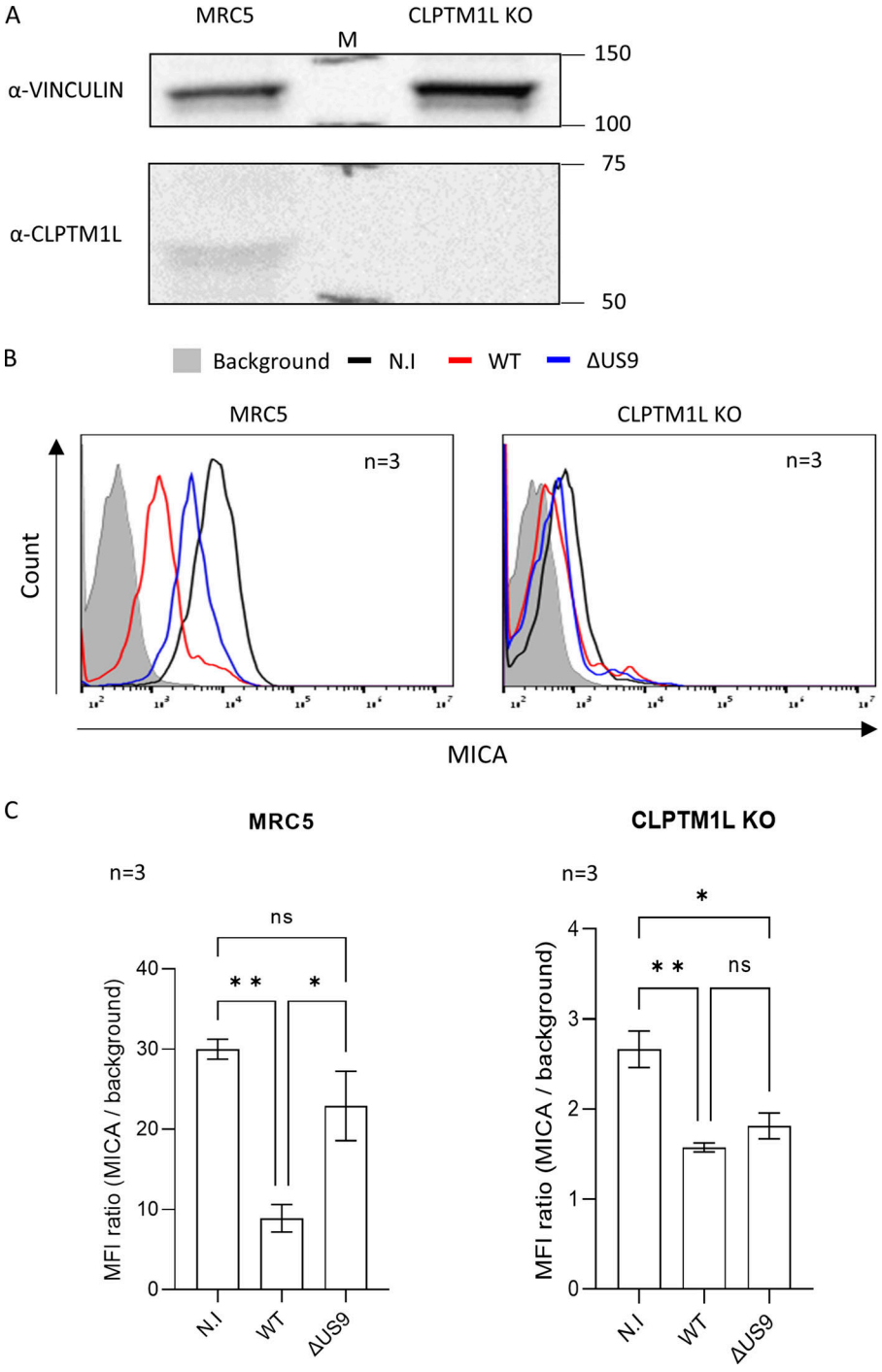

Figure 4. **MICA*008 is downregulated by US9 via CLPTM1L during HCMV infection. (A)** MRC-5 fibroblasts, either parental (MRC-5) or CLPTM1L KO, were lysed and analyzed by WB. Detection Abs are indicated on the left. M, protein ladder (marker). **(B)** Cells as in A were infected with AD169varL (WT, red line) or its previously generated US9 deletion mutant, ΔUS9 (Seidel et al., 2015; blue line). Uninfected cells were used as control (N.I, black line). At 72 hpi, the cells were stained with the indicated Abs, and FCM was performed. Isotype control was used as background (gray-filled histogram). **(C)** MFI quantification of MICA*008, calculated from two independent experiments as in B. Parental MRC-5 cells, left panel, CLPTM1L KO cells, right panel. For normalization, in each repetition the α-MICA MFI was divided by the background (secondary Ab only). A one-way ANOVA was performed separately for each cell type with a significant effect at the $P < 0.01$ level for all conditions (Parental MRC-5 ($F [2, 6] = 14.83$, $P = 0.0048$), CLPTM1L KO ($F [2, 6] = 15.26$, $P = 0.0044$)). A post-hoc Sidak's multiple comparison test was used to compare N.I to WT and ΔUS9, and WT to ΔUS9. Data shows mean and SEM. *, $P < 0.05$; **, $P < 0.01$; ns, non-significant.

for their surface expression, with MELTF being unique in its magnitude of downregulation. We also found that the expression of at least two other GPI-anchored proteins, ULBP2 and ULBP3, is CLPTM1L-independent, indicating that not all GPI-anchored proteins are CLPTM1L-dependent.

MELTF is downregulated by 9SP via CLPTM1L during HCMV infection

Having demonstrated that CLPTM1L KO affects at least three additional GPI-anchored proteins, we next wondered whether CLPTM1L-dependent proteins would be affected by US9, similar to MICA*008. Because the downregulation of MICA*008 by US9 was shown to be mediated by 9SP as well as other US9 domains (Seidel et al., 2021a), we also wanted to examine the isolated effect of each mechanism on the expression level of these CLPTM1L-dependent proteins. We presumed that CLPTM1L-dependent proteins would only be affected by 9SP, since CLPTM1L specifically precipitates with this domain (Fig. 2 D and Table S1 and Data S1).

We therefore analyzed the surface expression of CD109, CD59, and MELTF by FCM on RKO*008 EV, US9, and sw8SP cells (Fig. 6 A). We observed downregulation of all three proteins in

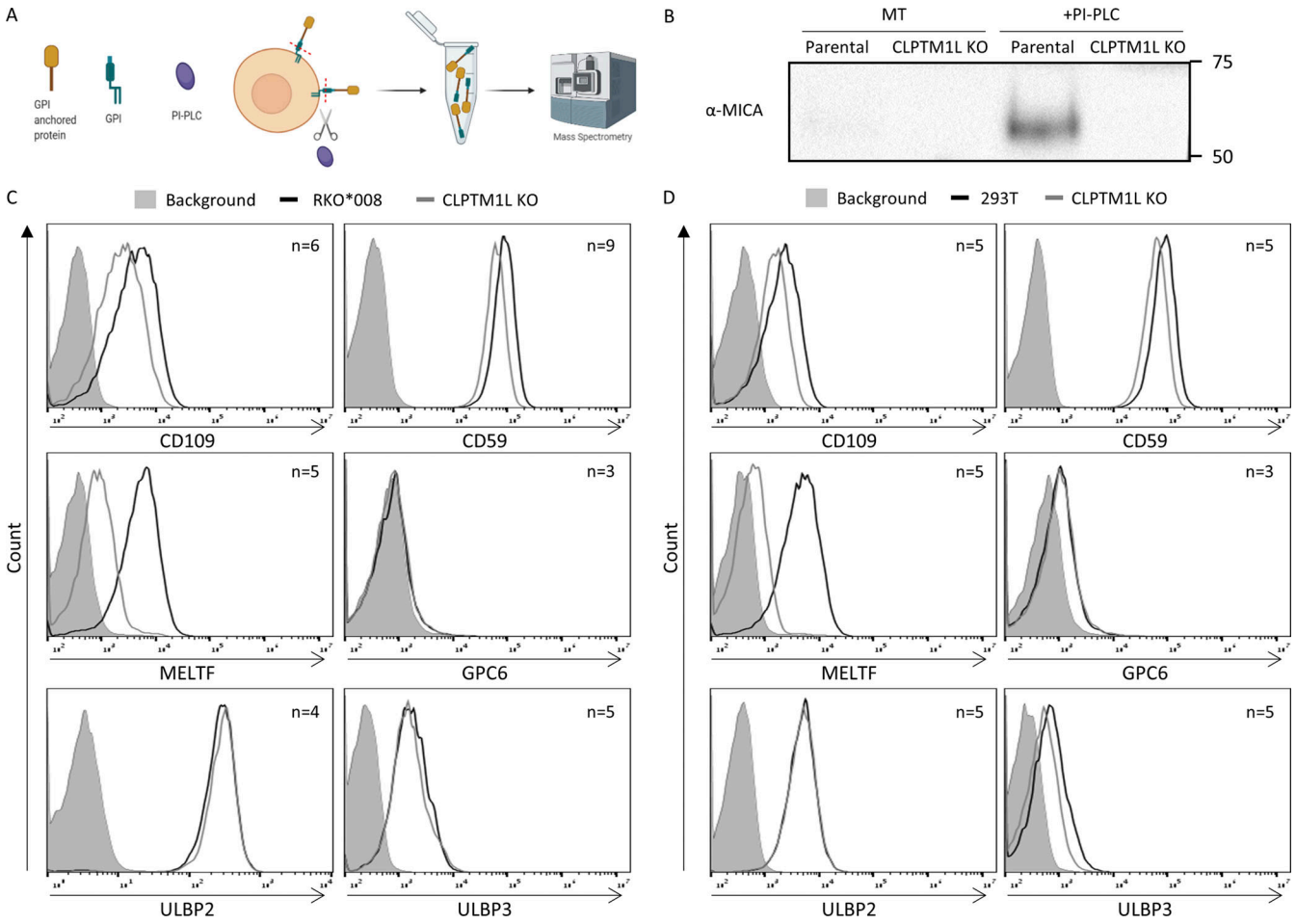

Figure 5. **CLPTM1L plays a role in the expression of additional GPI-anchored proteins. (A)** Cells of interest were incubated with PI-PLC at 37°C for 4 h. Cell media (containing cleaved GPI-anchored proteins) were then collected and sent to MS or used for WB analysis. **(B)** WB analysis performed on the supernatants which were sent to MS, for quality control. Detection Ab is α-MICA. MT, mock treated. **(C and D)** FCM of parental (black line) or CLPTM1L KO (gray line) cells was performed with the indicated Abs. Secondary Ab only or PE-conjugated isotype control (when appropriate) was used as background (gray-filled histogram). **(C)** Staining of RKO*008 cells. **(D)** Staining of 293T cells. Source data are available for this figure: SourceData F5.

US9-expressing cells to a similar extent to that observed in CLPTM1L KO cells. Importantly, these proteins were not downregulated in sw8SP-expressing cells, supporting the hypothesis that 9SP is necessary for US9's effect on CLPTM1L. To check if 9SP is also sufficient for US9's effect on CLPTM1L, we repeated this staining in RKO*008 EV, US8, and sw9SP cells. Indeed, while US8 did not affect the expression of any of these proteins, sw9SP successfully downregulated all three of them (Fig. 6 B).

Seeing that there was a resemblance between the effect of 9SP expression and CLPTM1L KO on the surface expression of the CLPTM1L-dependent GPI-anchored proteins, we wished to test whether similar results would be obtained during HCMV infection. Since MELTF was the most dramatically downregulated target, we chose to focus on this protein for further analysis.

To this end, we infected either parental or CLPTM1L KO MRC-5 fibroblasts with WT or ΔUS9 HCMV strains. The infected cells were harvested at 72 hpi, and the expression levels of MELTF were evaluated using FCM. The expression of MELTF in parental MRC-5 was higher upon ΔUS9 infection as compared with WT infection or N.I control (Fig. 6 C, left panel). This indicates that HCMV indeed downregulates MELTF via US9. Interestingly, in parental MRC-5, there was only minimal downregulation of MELTF in WT-infected cells as compared with N.I control (Fig. 6 C, left panel). In the CLPTM1L KO MRC-5 cells, MELTF expression was completely abolished (Fig. 6 C, right panel), suggesting great dependence on CLPTM1L in this cell type.

PIG-T interacts with CLPTM1L and is itself important for MICA*008 maturation and surface expression

We next wondered if CLPTM1L interacts with the TAC itself since CLPTM1L's KO seemed to inhibit the GPI-anchoring step for MICA*008 and possibly for the other identified proteins. To address this question, we performed a Co-IP assay using α-FLAG Ab in the RKO*008 Rescue C'FLAG cells and in RKO*008 KO EV for control. By LC-MS/MS, we found that CLPTM1L specifically precipitates with PIG-T (Table S2 and Data S3), an essential TAC member (Ohishi et al., 2003).

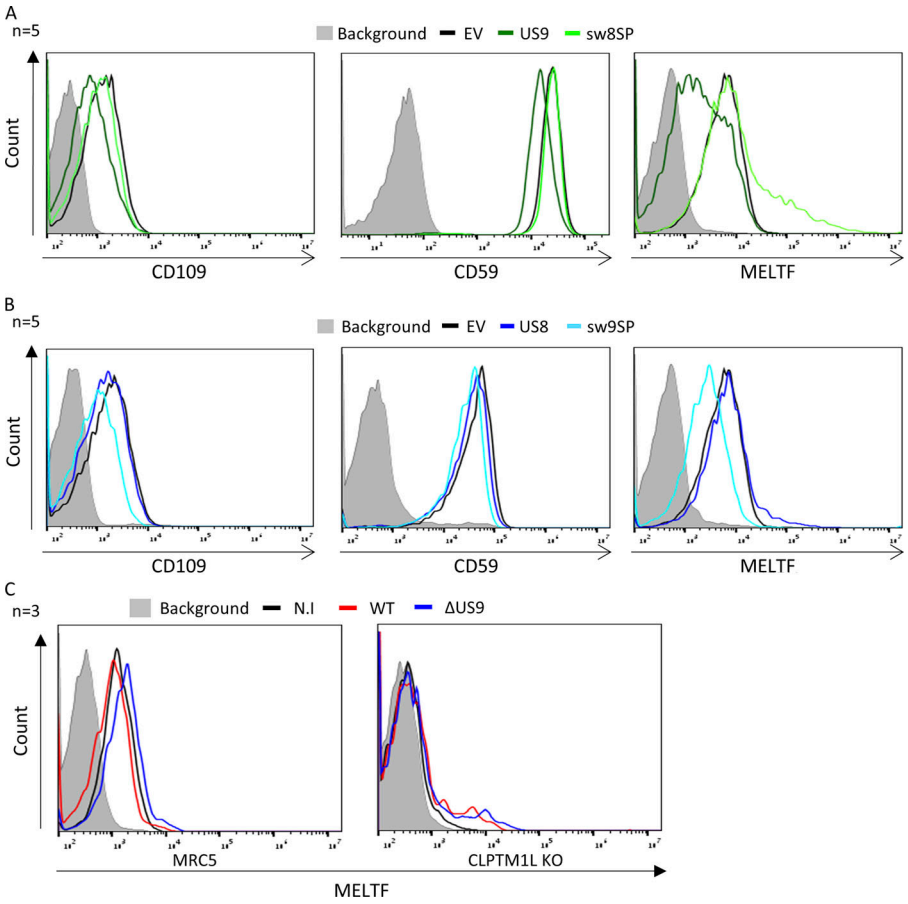

Figure 6. **MELTF is downregulated by 9SP via CLPTM1L during HCMV infection. (A)** RKO*008 cells co-expressing either an EV (black line), US9-HIS (US9, dark green line), or sw8SP-HIS (sw8SP, light green line) were stained with the indicated Abs. Secondary Ab only or isotype control (when appropriate) was used as background (gray-filled histogram). **(B)** RKO*008 cells co-expressing either an EV (black line), US8-HIS (US8, dark blue line), or sw9SP-HIS (sw9SP, light blue line) were stained with the indicated Abs. Secondary Ab only or isotype control (when appropriate) was used as background (gray-filled histogram). **(C)** MRC-5 fibroblasts, either parental (MRC-5) or CLPTM1L KO, were infected with AD169varL (WT, red line) or its previously generated US9 deletion mutant, ΔUS9 (Seidel et al., 2015; blue line). Uninfected cells were used as control (N.I, black line). At 72 hpi, the cells were stained with an α-MELTF Ab and FCM was performed. Secondary Ab only was used as background (gray-filled histogram).

We corroborated this finding by repeating the α-FLAG Co-IP experiment and performing a WB to specifically detect PIG-T in the IP eluates. Cell lysates before precipitation were used as input control, showing that PIG-T can be detected in both cell types, migrating at ∼65 kD (Fig. 7 A). Importantly, PIG-T was specifically detected in the Rescue C'FLAG IP eluates, indicating that CLPTM1L interacts with PIG-T (Fig. 7 B). To verify that the band detected in this experiment contained PIG-T, we repeated this experiment once more, this time using size-based separation to excise specific bands from the precipitation eluates which we sent for LC-MS/MS analysis. Indeed, PIG-T was specifically detected in the ∼65 KD band of the Rescue C'FLAG IP eluate, confirming that PIG-T precipitates with CLPTM1L (summarized in Table S3 and Data S4).

To investigate the possible involvement of PIG-T in the expression of CLPTM1L-dependent proteins, we knocked out PIG-T in 293T cells (Fig. 7 C). We then evaluated MICA*008 and MELTF surface expression levels in parental and KO 293T cells using FCM (Fig. 7 D, MICA, upper panel, MELTF, lower panel). The expression of both proteins was almost completely abolished, supporting our assumption that PIG-T is important for MICA*008 and MELTF's maturation and surface expression.

Based on these findings, we hypothesized that CLPTM1L functions as a facilitator of interactions between the TAC and its substrates. However, although the majority of PIG-T is known to be covalently bound to another TAC subunit, PIG-K (Ohishi et al., 2003), we could not detect PIG-K in the Rescue C'FLAG IP eluates in any of the experiments (Data S2, S3, and S4). To verify this, we performed another Co-IP assay, this time using a specific α-PIG-K Ab, in RKO*008 EV and US9 cells. Cell lysates before precipitation were used as input control, showing that CLPTM1L can be detected in both cell types (Fig. 7 E). Also in this experiment, we could not detect a CLPTM1L–PIG-K interaction (Fig. 7 F), suggesting that the PIG-T that is bound by CLPTM1L is not covalently bound to PIG-K ("free PIG-T").

Taken together, our results show that CLPTM1L is required to varying extents for GPI-anchoring of several proteins, including MICA*008 and MELTF. We also demonstrate that CLPTM1L interacts with free PIG-T, a known GPI-anchoring pathway component, supporting its role as a bona fide GPI-anchoring pathway constituent which is targeted by the HCMV protein US9.

US9 inhibits CLPTM1L's association with PIG-T

To investigate how US9 affects CLPTM1L, we initially tested whether it affects CLPTM1L expression level. We assumed that it does not influence CLPTM1L's protein levels since this would have been readily observed in WB in cells overexpressing US9 or 9SP (Fig. 2, A and C). To validate this, we infected MRC-5 fibroblasts with WT or ΔUS9 HCMV strains and harvested the infected cells at 72 hpi for WB analysis (Fig. S4 A). As expected, there was no difference in CLPTM1L's total levels between the WT and the ΔUS9-infected cells. There was, however, a similar downregulation of CLPTM1L in WT and ΔUS9-infected cells as

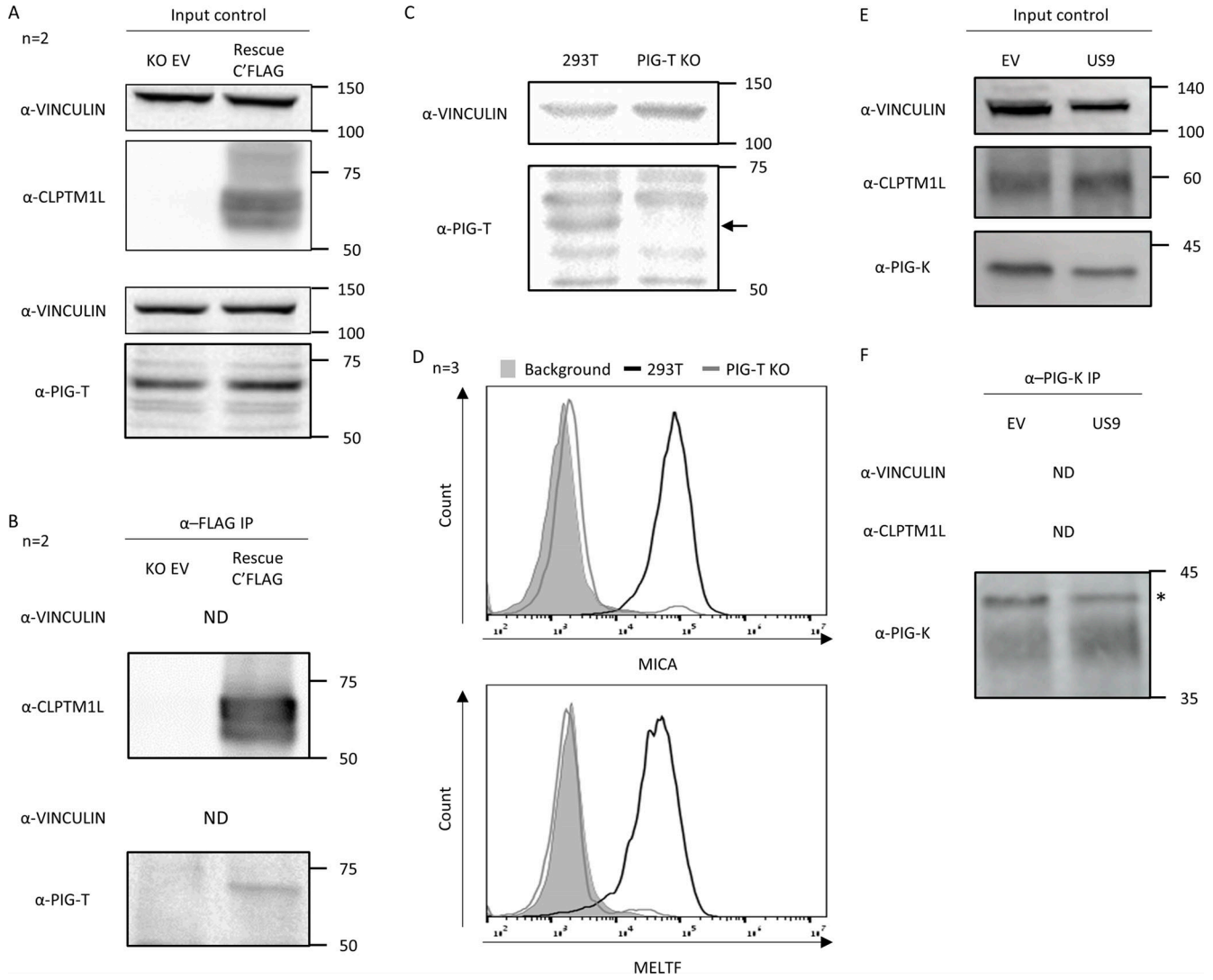

Figure 7. **PIG-T interacts with CLPTM1L and is itself involved in MICA*008 maturation and surface expression. (A and B)** Co-IP performed in RKO*008 CLPTM1L KO cells expressing an EV (KO EV) or a C'FLAG tagged CLPTM1L (Rescue C'FLAG). Detection Abs are indicated next to each blot; ND, not detected. **(A)** Cell lysates before precipitation were used as input control. **(B)** Precipitation Ab used was α-FLAG. **(C)** 293T cells, either parental (293T) or after PIG-T KO, were lysed and analyzed by WB. Detection Abs are indicated on the left. Arrow shows a specific PIG-T band (~65 kD). **(D)** Cells as in C were stained with the indicated Abs and analyzed by FCM. 293T, black line, PIG-T KO, gray line. Background (secondary Ab only), gray-filled histogram. **(E and F)** Co-IP performed in RKO*008 cells, co-expressing either EV or US9-HIS (US9). Detection Abs are indicated next to each blot. ND, not detected. **(E)** Cell lysates before precipitation were used as input control. **(F)** Precipitation Ab used was α-PIG-K. Asterisk indicates the specific PIG-K band (~42 kD). Source data are available for this figure: SourceData F7.

compared with N.I control, suggesting that it is modulated during HCMV infection either as a cellular response or by an unrelated viral mechanism.

We next utilized immunofluorescence (IF) imaging to see if US9 alters CLPTM1L's cellular localization to hinder its activity. We fixed RKO*008 and RKO*008 US9-HIS cells and stained them for HIS tag and CLPTM1L. Nuclei were counterstained with DAPI. In both cell types, CLPTM1L was detected mainly around the nuclei, strongly correlating with its known localization to the ER (Fig. S4 B). Due to the lack of change in CLPTM1L's staining, we concluded that US9 does not affect CLPTM1L's localization.

Finally, we speculated that US9 may act to inhibit CLPTM1L's interaction with either PIG-T or its substrates (such as MICA*008). We suspected the former because we could not detect MICA*008 by MS in the IP eluates of any of the α-FLAG IP experiments we had performed (Data S2, S3, and S4). Furthermore, when we repeated the α-FLAG Co-IP experiment and specifically looked for MICA*008 by WB, we still did not see it co-precipitate (Fig. S4 C). This suggests that CLPTM1L facilitates GPI-anchoring without directly interacting with the GPI-anchored proteins themselves, or perhaps, that the interaction is too transient or too weak to detect and investigate.

We were therefore left with the possibility that US9 physically inhibits CLPTM1L's interaction with PIG-T. To check this, we used the Rescue C'FLAG cells we had generated and co-expressed our US9-HIS construct in them ("Rescue + US9"). We then performed a Co-IP assay using α-FLAG Ab in the Rescue

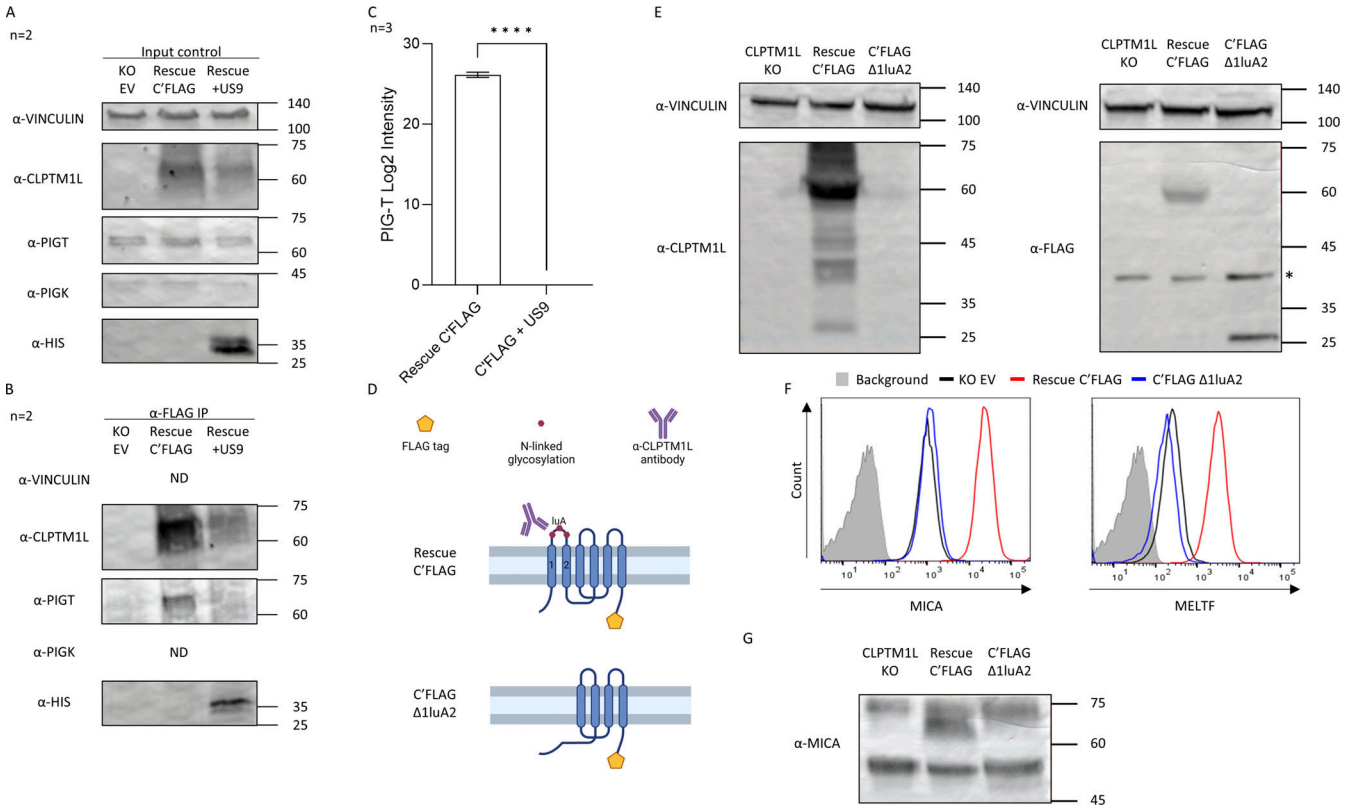

Figure 8. **US9 inhibits CLPTM1L's association with the TAC. (A and B)** Co-IP performed in RKO*008 CLPTM1L KO cells expressing an EV (KO EV), a C'FLAG tagged CLPTM1L (Rescue C'FLAG), or both a C'FLAG tagged CLPTM1L and US9-HIS (Rescue + US9). KO EV cells were used as a negative control for the IP. Detection Abs are indicated next to each blot; ND, not detected. **(A)** Cell lysates before precipitation were used as input control. **(B)** Precipitation Ab used was α-FLAG. **(C)** Co-IP was performed as in A and B. Instead of detection by WB, IP eluates were sent for MS analysis to evaluate PIG-T intensity levels. Column bar graph shows mean and SEM for three biological replicates, for Rescue C'FLAG, and Rescue + US9 cells. PIG-T was not detected in the negative control, KO EV cells. ****P < 0.0001, unpaired two-tailed *t* test. **(D)** A scheme showing selected features of CLPTM1L's structure. CLPTM1L possesses 5–8 TM domains (here showing six). α-CLPTM1L Ab is directed against a large amino acid sequence in the first luminal domain (luA), which is located between TM1 and TM2. This domain has N-linked glycosylations in three positions. In Rescue C'FLAG cells, CLPTM1L has a C-terminal cytosolic FLAG tag. In C'FLAG Δ1luA2 cells, CLPTM1L is mutated and the luA domain is absent, along with TM1 and TM2 domains. Its cytosolic N-terminal end is fused to the rest of the protein, and its cytosolic C-terminus contains a FLAG tag. **(E)** RKO*008 CLPTM1L KO, Rescue C'FLAG, or C'FLAG Δ1luA2 cells were lysed and analyzed by WB. Detection Abs are indicated next to each blot. Asterisk indicates 3XFLAG peptide originating from the PX459 vector used to carry out the CLPTM1L KO. **(F)** RKO*008 KO EV, Rescue C'FLAG, or C'FLAG Δ1luA2 cells were stained with indicated Ab and analyzed by FCM. KO EV, black line, Rescue C'FLAG, red line, C'FLAG Δ1luA2, blue line. Background (secondary Ab only), gray-filled histogram. **(G)** Cells as in E were lysed and analyzed by WB; detection Ab is indicated next to the blot. Loading control is the same as in the right panel of E; the membrane was reblotted with α-MICA Ab after destaining.

C'FLAG and the Rescue + US9 cells and in the KO EV cells for control. Cell lysates before precipitation were used as input control, showing that PIG-T can be detected in all cell types and that US9 is expressed in the Rescue + US9 cells (Fig. 8 A). In concordance with our speculation, we detected a specific PIG-T band only in the Rescue C'FLAG cell eluate, implying that US9 interferes with the CLPTM1L-PIG-T interaction (Fig. 8 B). In this experiment, which also reciprocally validated CLPTM1L's interaction with US9, predominantly the larger SP^+ form of US9 co-precipitated with CLPTM1L (Fig. 8 B). To corroborate these findings, we repeated this Co-IP experiment three times, each time analyzing the results by LC-MS/MS. Indeed, PIG-T could only be detected in the Rescue C'FLAG IP eluates (quantified in Fig. 8 C and Data S5).

Interestingly, when we attempted to precipitate CLPTM1L using a commercial polyclonal α-CLPTM1L Ab (HPA014791), although we successfully precipitated CLPTM1L, neither US9 nor PIG-T was detected in the IP eluates (Fig. S5, A and B). We therefore hypothesized that both US9 and PIG-T bind the same region in CLPTM1L, which is blocked by the specific Ab we used. CLPTM1L's structure is predicted to have 5–8 TM domains, with both of its C- and N-terminal domains located on the cytoplasmic side of the ER (Wang et al., 2022). Its first ER luminal domain (termed "luA") is rather long (252 amino acids) and contains three N-linked glycosylations, making it more likely to be involved in protein–protein interactions (Fig. 8 D). Importantly, the epitope sequence used to generate the commercial polyclonal Ab comprises more than half (~0.54) of the amino acids that compose the luA domain (Fig. 8 D and Fig. S5 C). Based on these results, we next studied the functional importance of the luA domain. We therefore generated a Δ1luA2 CLPTM1L construct, which is missing the entire luA domain and the two adjacent TM domains to preserve proper protein orientation (Fig. 8 D), and expressed it in RKO*008 CLPTM1L KO cells. Since the

α-CLPTM1L Ab would not be able to detect this mutant in WB assays, the construct was designed to contain a C-terminal FLAG tag ("C'FLAG Δ1luA2"), similar to the full CLPTM1L rescue construct. Indeed, we could use an α-FLAG Ab to validate the proper expression of this protein (Fig. 8 E, right panel), while the α-CLPTM1L could not detect it, confirming that it does not contain the luA domain (Fig. 8 E, left panel). Using FCM, we then evaluated the surface levels of MICA*008 and MELTF in the C'FLAG Δ1luA2 cells. For controls, we used Rescue C'FLAG and KO EV cells. In agreement with our hypothesis, the C'FLAG Δ1luA2 completely failed to restore the surface levels of both proteins (Fig. 8 F), phenocopying the KO EV cells.

Next, we wanted to validate that in C'FLAG Δ1luA2 cells, MICA*008 levels are not restored due to Δ1luA2 CLPTM1L's inability to facilitate GPI-anchoring. To show this, we lysed KO EV, Rescue C'FLAG, and C'FLAG Δ1luA2 cells, and analyzed the various MICA*008 forms by WB. Previously, we showed that CLPTM1L depletion leads to a specific reduction in the post-ER mature GPI$^+$ form of MICA*008 (Fig. 3, E–G), and that this form is restored in the Rescue C'FLAG cells. In C'FLAG Δ1luA2 cells, there was no change in the post-ER mature GPI$^+$ form of MICA*008 as compared with CLPTM1L KO cells (Fig. 8 G), supporting GPI-anchoring properties of the luA domain of CLPTM1L.

Discussion

In recent years, the importance of the GPI-anchoring pathway in human health has become increasingly apparent due to accumulating evidence that constituents of this pathway and the resultant GPI-anchored proteins are key to immune modulation and normal development (Hussein et al., 2020; Manea, 2018; Gennarini et al., 2017; Kinoshita, 2020). The pathway includes biosynthesis of the GPI moiety, cleavage of precursor proteins and attachment to the GPI moiety by the TAC, remodeling of the nascent GPI-anchored proteins, and protein transport to the cell surface via the Golgi apparatus.

Here, we have shown that 9SP binds CLPTM1L to downregulate MICA*008 expression. We found that CLPTM1L is a key factor in the poorly understood GPI-anchoring of MICA*008, and in its absence, surface MICA*008 expression is reduced. We further verified that during HCMV infection, US9 acts via CLPTM1L to downregulate MICA*008.

It has been theorized that MICA*008 is processed by a non-standard GPI-anchoring pathway (Seidel et al., 2021a; Ashiru et al., 2013; Seidel et al., 2015) due to its unusually slow maturation kinetics (Ashiru et al., 2013) and the inability of prediction tools which existed at the time (such as PredGPI [Pierleoni et al., 2008]) to identify a MICA*008 GAS. A recently published recurrent neural network–based prediction tool called NetGPI 1.1 (Gíslason et al., 2021) does, however, predict MICA*008 to be GPI-anchored, with the S residue at position 313 as the ω-site. MICA*008 is unique also because it is first synthesized as a soluble protein, departing from the canonical view that proteins destined for GPI-anchoring are associated with the ER membrane until attachment takes place (Kinoshita and Fujita, 2016). On the other hand, this theory has been challenged by evidence showing that soluble proteins can be GPI-anchored as well, much like MICA*008 itself (Galian et al., 2012).

We discovered here that the expression of at least three other GPI-anchored proteins (CD109, CD59, and MELTF) is, to varying extent, CLPTM1L-dependent. Intriguingly, we found that two other GPI-anchored proteins, ULBP2 and ULBP3, are not affected by CLPTM1L KO. Indeed, we have shown here that when MICA*008 is attached to a canonical GAS (the MICA*008-3TM mutant, with the GAS of ULBP3), it becomes US9 resistant (Seidel et al., 2015) and CLPTM1L-independent. These observations support a variable function of CLPTM1L, which is also GAS-dependent.

We showed that all three CLPTM1L-dependent proteins are downregulated by 9SP, and not by other US9 domains, indicating that 9SP alone is necessary for inhibition of CLPTM1L's function. We also found that MELTF, which strongly depends on CLPTM1L for its surface expression, is downregulated by US9 during HCMV infection, likely via CLPTM1L.

Functionally, MELTF is involved in transferrin-independent uptake of iron (Kennard et al., 1995), an essential element to many biological processes (Muckenthaler et al., 2017). Iron levels are closely monitored to prevent cellular damage (Muckenthaler et al., 2017; Yang et al., 2020), so it is unsurprising that HCMV benefits from modulation of the iron-metabolism pathway (Sun et al., 2018; Vahdati-Ben Arieh et al., 2003; Georgopoulou et al., 2014; Martin et al., 2022). We showed here that MELTF is only minimally downregulated in WT HCMV-infected cells as compared with N.I controls, suggesting upregulation of MELTF as a cellular response to viral infection. It is therefore possible that MELTF's downregulation is beneficial to HCMV, either due to its metabolic function or due to a more direct inhibitory role. MELTF's possible immunological function will therefore be explored in the future.

We discovered here that CLPTM1L binds PIG-T, which has a central role in the stabilization of the TAC (Ohishi et al., 2003), possibly regulating access to its catalytic site (Eisenhaber et al., 2003). Based on this, we hypothesized that CLPTM1L may facilitate interactions between the TAC and its substrates. Interestingly, we found that although PIG-T is known to share a disulfide bond with PIG-K, the latter did not co-precipitate with CLPTM1L. This suggests that the PIG-T form bound by CLPTM1L is not covalently linked to PIG-K. It does not necessarily mean, however, that this free PIG-T executes a function unrelated to the TAC, as it was previously shown that even when preventing the formation of the PIG-K–PIG-T bond, the TAC is still able to form and it retains some GPI-anchoring functionality (Ohishi et al., 2003). Moreover, the TAC structure has only very recently been resolved, with two different structural maps found (Zhang et al., 2022). Unfortunately, one of the two was not resolved with high resolution, so there is no information regarding the presence or absence of a PIG-K–PIG-T disulfide bond in it.

Finally, we have shown that US9 inhibits CLPTM1L's binding to PIG-T and that the accessibility of CLPTM1L's luA domain is important for US9 binding. Based on these findings, we hypothesize that 9SP acts by binding the 1luA2 region, thereby preventing its binding to PIG-T.

A recent genome-wide CRISPR screen (Wang et al., 2022) identified CLPTM1L as a lipid scramblase, translocating the second GPI intermediate (glucosaminyl-phosphatidylinositol, GlcN-PI) from the cytosolic to the luminal face of the ER membrane. The authors modeled CLPTM1L and found that it shares homology with two SWEET/PQ-loop family members, which are metabolite transporters. In support of our own findings, the authors also observed a moderate and cell-type-dependent downregulation of CD59 in the absence of CLPTM1L, which they attribute to the functional redundancy with other, as-yet-unidentified scramblases.

While this report supports our findings regarding CLPTM1L's involvement in the GPI-anchoring pathway, our results regarding CLPTM1L's binding to PIG-T suggest that CLPTM1L may not function solely as a GlcN-PI scramblase. First, because this process occurs early in GPI-moiety synthesis when no interaction with a TAC component is expected. Second, because we have shown here that the 1luA2 region is crucial for the GPI-anchoring function of CLPTM1L and that its accessibility is important for PIG-T binding. Inspection of the sequence alignment and structure comparison between CLPTM1L and its other homologous SWEET/PQ-loop family members reveals that the TM1 and luA domains are unique to CLPTM1L and is completely absent in its homologs (Wang et al., 2022), suggesting that these domains may have non-scramblase functions. Finally, not all proteins are CLPTM1L-dependent, which could be explained by differential sensitivity to GPI moiety abundance determined by scramblase activity (i.e., some proteins are preferentially anchored when GPI moiety abundance is low). Nonetheless, it is difficult to explain MICA*008's extreme dependence on CLPTM1L across multiple tested cell types (Seidel et al., 2015; Seidel et al., 2021a) merely by effects on downstream GPI moiety availability. One could speculate that due to MICA*008's slow maturation kinetics, further GPI-anchoring delay that occurs under limited GPI moiety conditions results in increased MICA*008 degradation by the ERAD. Ruling out this possibility, we have previously shown that even when preventing MICA*008's degradation, it is still not GPI-anchored in US9 expressing cells, but instead, it is retained in the ER in a non-GPI-anchored form (Seidel et al., 2021a).

Unfortunately, we could not test the isolated effect of potential downstream functions of CLPTM1L because these would be affected by the abundance of the GPI moiety in the ER, which is in turn affected by the scramblase activity. Either way, future research is needed to explore the effect of GPI moiety abundance on the GPI-anchoring efficiency of different proteins and to ascertain whether there are other potential CLPTM1L functions affecting MICA*008 or other GPI-anchored proteins.

It remains unclear what makes a GPI-anchored protein CLPTM1L-dependent. As discussed above, it seems to depend, at least partially, on the GAS, since the MICA*008-3TM mutant is CLPTM1L-independent. Taken together, we present two potential models for CLPTM1L's function: According to one model (Fig. 9 A), CLPTM1L's 1luA2 region binds to free PIG-T and promotes TAC recognition of a subset of GPI-anchored proteins. The same subset is downregulated upon HCMV infection due to 9SP's inhibition of the PIG-T–CLPTM1L association, which results in decreased TAC processing. Whether US9 influences CLPTM1L's scramblase activity as well remains unclear. Alternatively (Fig. 9 B), free PIG-T may bind the 1luA2 region to positively regulate CLPTM1L's scramblase function. 9SP inhibits this positive regulation, thus reducing GPI moiety abundance in the ER lumen. A subset of GPI-anchored proteins that are sensitive to these conditions, remain unanchored and may subsequenty be degraded.

In conclusion, we have shown here that 9SP targets a novel GPI-anchoring pathway component, CLPTM1L, as we previously speculated (Seidel et al., 2015, 2021a). This interaction was also observed in recently published HCMV interactome data (Nobre et al., 2019). This elegant mechanism enables HCMV to block the expression of a major activating immune ligand through the use of an uncharacteristically short peptide of just 27 amino acids (Halenius et al., 2015; De Pelsmaeker et al., 2018). We harnessed this unique interaction as a tool for the discovery of CLPTM1L, a hitherto-uncharacterized component of the GPI-anchoring pathway, as well as three of its downstream targets, CD109, CD59, and MELTF. This discovery sheds light both on basic aspects of cell biology as well as on the sophistication with which viruses manipulate the immune response.

Materials and methods

Cells and Abs

293T (CRL-3216), RKO (CRL-2577), and HeLa (CCL-2) cells were grown in DMEM (Sigma-Aldrich) containing 10% FBS (Sigma-Aldrich), 1% *L*-glutamine (Biological Industries [BI]), 1% sodium pyruvate (BI), 1% nonessential amino acids (BI), and 1% penicillin-streptomycin (BI). MRC-5 primary lung fibroblasts (CCL-171) were grown in EMEM media with the same supplements and were used below passage 20.

We used the following primary Abs for FCM: Mouse α-human MICA (cat. MAB1300; R&D Systems), mouse α-human CD109 (cat. 323306; BioLegend), mouse α-human CD59 (cat. 304707; BioLegend), mouse α-human MELTF (cat. MAB81751; R&D Systems), mouse α-human GPC6 (cat. MAB2845; R&D Systems), mouse α-human ULBP2/5/6 (cat. MAB1298; R&D Systems), and mouse α-human ULBP3 (cat. MAB1517; R&D Systems). We used the following isotype controls for FCM: Mouse IgG1 (cat. 400112; BioLegend) and mouse IgG2a (cat. 400212; BioLegend).

The following secondary Abs were used for FCM: Goat α-mouse (cat. 115-606-062; Jackson ImmunoResearch Laboratories) and goat α-rabbit IgG (cat. 111-606-144; Jackson ImmunoResearch Laboratories).

We used the following primary Abs for WB: mouse α-HIS tag (cat. MAB050; R&D systems), rabbit α-human MICA (cat. ab150355; Abcam), rabbit α-Vinculin (cat. ab129002; Abcam), rabbit α-human CLPTM1L (cat. HPA014791; Sigma-Aldrich), rat α- FLAG tag (cat. 637302; BioLegend), rabbit α-PIGT (cat. 14–266; ProSci), and rabbit α-PIGK (cat. ab201693; Abcam). The α-HIS, α-FLAG tag, α-PIG-K, and α-CLPTM1L Abs were also used for Co-IP. The mouse α-HIS and α-CLPTM1L Abs were also used for IF.

The following secondary Abs were used for WB: Goat α-rabbit (cat. 111-035-144; Jackson ImmunoResearch Laboratories) and goat α-rat (cat. 112-035-062; Jackson ImmunoResearch Laboratories). For WB of Co-IP lysates, the following secondary

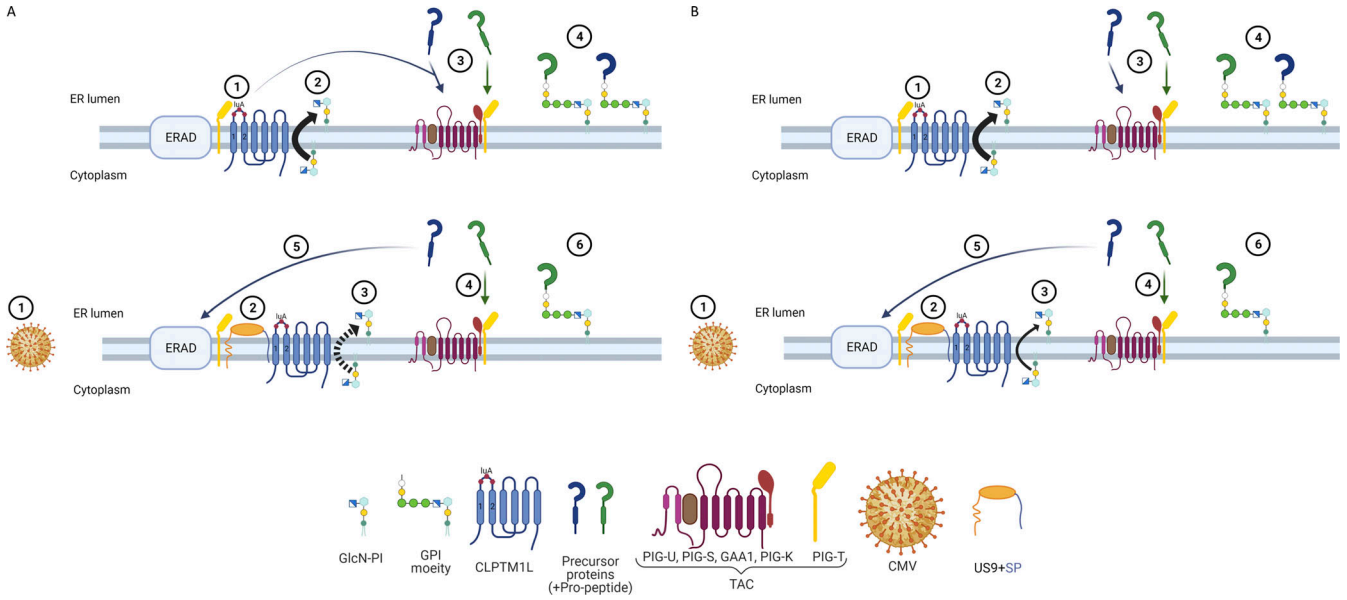

Figure 9. **Two models for CLPTM1L's function. (A)** Upper panel: **(1)** CLPTM1L's 1luA2 region binds to free PIG-T, promoting TAC processing of a subset of precursor proteins (blue line). **(2)** GPI moiety abundance in the ER lumen is determined by the scrambling extent of GlcN-PI by CLPTM1L and additional proteins which act redundantly (thick black arrow). **(3)** All precursor proteins are processed by the TAC (blue and green arrows). **(4)** Nascent GPI-anchored proteins are ready to be modified and transported to the cell surface via the Golgi apparatus. Lower panel: **(1)** HCMV infects host cells. **(2)** US9 is expressed, and 9SP interrupts the PIG-T–CLPTM1L association, thus inhibiting CLPTM1L's 1luA2 region. **(3)** The extent of GlcN-PI scrambling is unknown (dashed black arrow). **(4)** Most precursor proteins are CLPTM1L-independent, meaning they are unaffected by its inhibition and are therefore still processed by the TAC (green arrow). **(5)** A subset of precursor proteins which is CLPTM1L-dependent is not processed by the TAC and is sent to degradation via the ERAD machinery instead (blue arrow). **(6)** The result is selective downregulation of a specific subset of CLPTM1L-dependent, GPI-anchored proteins. **(B)** Upper panel: **(1)** CLPTM1L is a GlcN-PI scramblase positively regulated by PIG-T's binding to CLPTM1L's 1luA2 region. **(2)** GPI moiety abundance in the ER lumen is determined by the extent of GlcN-PI scrambling by CLPTM1L and additional proteins which act redundantly (thick black arrow). **(3)** All precursor proteins are processed by the TAC, albeit with different efficiencies (blue and green arrows). **(4)** Nascent GPI-anchored proteins are ready to be modified and transported to the cell surface via the Golgi apparatus. Lower panel: **(1)** HCMV infects host cells. **(2)** US9 is expressed, and 9SP interrupts the PIG-T–CLPTM1L association, thus inhibiting CLPTM1L's scramblase activity. **(3)** GlcN-PI is scrambled to a lesser extent due to inhibition of CLPTM1L (thin black arrow), resulting in low GPI moiety abundance. **(4)** Precursor proteins which are efficiently processed by the TAC are unaffected by the changed conditions and are therefore still processed (green arrow). **(5)** Precursor proteins which are inefficiently processed by the TAC are sensitive to the decreased GPI moiety availability. In these conditions, these proteins are not processed, and are sent to degradation via the ERAD machinery instead (blue arrow). **(6)** The result is selective downregulation of a specific subset of GPI-anchored proteins.

Abs were used: goat α-mouse, light chain specific (cat. 115-035-174; Jackson ImmunoResearch Laboratories), mouse α-rabbit, light chain specific (cat. 211-032-171; Jackson ImmunoResearch Laboratories), and goat α-rat IgG, light chain specific (cat. 112-035-175; Jackson ImmunoResearch Laboratories).

The following secondary Abs were used for IF: Alexa Fluor 647 donkey α-rabbit (cat. 711-605-152; Jackson ImmunoResearch Laboratories), Alexa Fluor 488 donkey α-mouse (cat. 715-546-151; Jackson ImmunoResearch Laboratories).

Plasmid transfection, lentiviral transduction, and CRISPR KO

The generation of RKO*008, RKO*004, and RKO*008-ULBP3TM cells and of the US9-HIS, sw8SP-HIS, US8-HIS, and sw9SP-HIS constructs were previously described (Seidel et al., 2015; Seidel et al., 2021a). Transfection reagent used in all transfections mentioned below is TransIT-LT1 (cat. MC-MIR-2300; Mirus Bio). Transfections were executed according to the manufacturer's instructions, except MRC-5 cells, which were plated a day ahead in a 75-ml flask.

All gRNAs were designed using the Broad Institute GPP sgRNA Design tool (now updated to the CRISPick tool https://portals.broadinstitute.org/gppx/crispick/public).

For CLPTM1L KO in RKO*008 cells, gRNAs were generated using PCR annealing of the following primers (listed from 5′ to 3′):

gRNA#1

Fw: 5′-phosphate(P)-CACCGTGAGCGTGTACACCACGACG-3′.

Rev: 5′-P-AAACGTCGTGGTGTACACGCTCAC-3′.

gRNA#2

Fw: 5′-P-CACCGATGCCGTACATGACCCAGC-3′.

Rev: 5′-P-AAACGCTGGGTCATGTACGGCATC-3′.

The annealed gRNAs were cloned into PX459V2.0-eSpCas9(1.1) plasmid (#108292; Addgene) vector using the BbsI restriction site, and the success of the ligation was validated with DNA sequencing. For CLPTM1L KO in RKO*004 and 293T cells, only gRNA#1 was used, after establishing in RKO*008 cells that both gRNAs functioned similarly. For CLPTM1L KO in MRC-5 and RKO*008-ULBP3TM cells, gRNA#2 was cloned into Lenti-CRISPR (pXPR_001) vector (Shalem et al., 2014) using the BsmBI restriction site, and the success of this ligation was validated with DNA sequencing as well.

For PIG-T KO, gRNAs were generated using PCR annealing of the following primers (listed from 5′ to 3′):

Fw: 5′-P-CACCGGGAGTCGATGAAGTTGAGAG-3′.

Rev: 5′-P-AAACCTCTCAACTTCATCGACTCCC-3′.

For RKO and 293T transfectants, 24 h after the transfections, selection with Puromycin-containing medium (5 µg/ml, cat. MBS540222; Calbiochem) was applied for 24–48 h. Clones of KO cells were achieved by plating the cells in 96U-well plates at a concentration of 2 cells/well. For MRC-5 transfectants, the selection with Puromycin (6 µg/ml) was applied for a week to maximize the number of cells with complete CLPTM1L KO in the culture.

The Rescue C'FLAG and Rescue N'FLAG constructs were generated using PCR amplification and were then cloned into a pHAGE DsRED^{-} eGFP^{+} vector under a CMV promotor using the XhoI and AgeI restriction sites. The following primers were used (listed from 5′ to 3′):

Rescue C'FLAG

Fw: 5′-ATCTCTCGAGGCCGCCACCATGTGGAGCGGCCGCAG CT-3′.

Rev: 5′-ATACCGGTTCACTTGTCGTCATCGTCTTTGTAGTCG TCCGTGTGGGGCGCCC-3′.

Rescue N'FLAG

Fw: 5′-ATCTCTCGAGGCCGCCACCATGGACTACAAAGACGA TGACGACAAGTG GAGCGGCCGCAGCTC-3′.

Rev: 5′-CCAGCCAAGTGCAACTTGAATTACCGGTAT-3′.

The C'FLAG Δ1luA2 construct was ordered from Twist Bioscience as a synthetic sequence cloned into the pHAGE DsRED^{-} eGFP^{+} vector under the same CMV promotor.

The resultant plasmids were then validated by DNA sequencing and used in a transient three-plasmid transfection to produce lentiviral vectors, as described previously (Stern-Ginossar et al., 2007; Seidel et al., 2021a).

FCM

In most cases, EDTA was used for harvesting the cells; otherwise, trypsin was used. In most cases, cells were plated at equal concentrations and incubated overnight prior to staining (because endogenous MICA is sensitive to contact inhibition). Resuspended cells were incubated on ice with the conjugated Abs for 0.5 h at a concentration of 0.5 µg/well and with unconjugated Abs for 1 h at the recommended concentrations by the company. Cells were incubated with secondary Abs for 0.5 h on ice at the recommended concentrations by the company. Cell-size-based gating was performed to achieve gating over living cell populations only.

WB

Cell lysates were prepared with a lysis buffer containing 0.6% SDS, 1% Aprotinin, 1 mM PMSF, and 10 mM TRIS [pH 7.4]. When indicated, lysates were digested with Endo H and PNGase F (cat. P0702L and P0704L, respectively; New England BioLabs), according to the manufacturer's instruction, under denaturing reaction conditions. Mock-treated lysates were treated according to the PNGase F protocol, with double-distilled water substituting the enzyme. Size-based separation was performed using 10, 12.5, or 15% SDS-PAGE, and was followed by blotting the proteins onto nitrocellulose membranes. The membranes were incubated for 1 h in blocking solution (Tween 0.4%, 5% skim milk in PBS X1) and were then stained with indicated primary Abs (diluted in 5% BSA, 0.05% sodium azide, Tween 0.4% in PBS X1) overnight at 4°C. The following day, membranes were 3× washed with Tween 0.4% in PBS X1 and then incubated with appropriate secondary Ab (diluted in the blocking solution) for 30 min. Membranes were finally 3× washed and then developed using ECL (cat. 20-500-500, BI, or cat. 32106; Thermo Fisher Scientific [TFS]). In certain cases, stripping of the membrane was performed to allow staining with a different Ab. To do this, membranes were incubated for 5–20 min in 0.2 M NaOH and then washed and reblocked. After verifying the absence of previously demonstrated bands, reblotting was performed. Images were acquired with the Image lab software (Bio-Rad) or with the FUSION FX Spectra software (Vilber). Quantification was performed only with the former.

Co-IP

Co-IP was performed as previously described (Seidel et al., 2021a). Briefly, cells were incubated overnight at concentrations ranging between 7 and 10 M in a 10-cm plate. The cells were washed and lysed for 30 min on ice with 1 ml of either NP40 buffer (50 mM Tris [pH 7.4], 2 mM EDTA, 0.05 mM sodium orthovandate, 1% mammalian protease inhibitor cocktail), or 1% digitonin buffer (150 mM NaCl, 50 mM Tris [pH 7.4], 1% mammalian protease inhibitor cocktail). The NP40 buffer was used in the case of the α-HIS IP with detection for MICA, and digitonin buffer was used in all other cases. For the α-HIS IP used for MS, cells were incubated prior to lysis for 3 h at 37°C with 2–4 µM epoxomicin.

Supernatants were precleared using an isotype control and protein G-plus beads and input controls were taken from the precleared supernatants. The latter was then mixed with the indicated precipitation Ab for 1 h and then protein G-plus beads were added (we used 4 µl α-HIS Ab with 40 µl beads, 6 µl α-FLAG Ab with 30 µl beads, 15 µl α-PIG-K Ab with 60 µl beads, and 30 µl α-CLPTM1L Ab with 30 µl beads). After overnight incubation at 4°C, the beads were washed and used for MS. Alternatively, beads were boiled in 2X protein sample buffer for 3 min to elute bound proteins to be used in size-based separation in SDS-PAGE. Following size-based separation, the gels were used for WB analysis. For the α-FLAG IP, a second gel was used for MS analysis after staining with InstantBlue Coomassie protein stain (1SB1L, cat. ab119211; Abcam), excision of specific bands, and destaining with 30% acetic acid and 10% ethanol.

Proteolysis and MS analysis of Co-IP experiments

Uneluted beads or specific gel bands were shipped at 4°C for proteolysis and MS analysis at the Smoler Proteomics Center, Technion Institute of Technology.

Uneluted beads were eluted in 100 µl 8 M urea and 100 mM ammonium bicarbonate (NH_4HCO_3) for 30 min with mild agitation in RT. The samples were centrifuged for 10 min at 10,000 *g* at RT and the supernatant was transferred to a new tube. DTT was added at a final concentration of 11 mM and the proteins were reduced at 60°C for 30 min with mild agitation, modified with 37.5 mM iodoacetamide and 100 mM NH_4HCO_3 (RT for 30 min in the dark). The samples were diluted to 1.5 M urea and the proteins were digested overnight at 37°C with

modified trypsin (Promega) at a 1:50 enzyme-to-substrate ratio under the assumption there is ~10 µg protein.

Specific protein gel bands were reduced with 3 mM DTT (60°C for 30 min), modified with 10 mM iodoacetamide in 100 mM NH_4HCO_3 (RT for 30 min in the dark), and digested in 10% acetonitrile and 10 mM NH_4HCO_3 with modified trypsin at a 1:10 enzyme-to-substrate ratio overnight at 37°C. Additional second trypsinization at a 1:20 enzyme-to-substrate ratio was performed for 4 h.

In all cases (uneluted beads and specific protein gel bands), after tryptic digestion, peptides were desalted using C18 tips (Homemade stage tips) and analyzed by LC-MS/MS. Results were analyzed vs. the human Uniprot database and against decoy databases (to determine the false discovery rate). Results were also analyzed vs. specific sequences (such as US9 or PI-PLC). All the identified peptides were filtered with 1% false discovery rate threshold and minimum of two peptides. A protein identified with a single unique peptide was not considered a certain identification. Known contaminants were also excluded. Where there was no signal detected, the value 0 was replaced with the minimal limit of detection for that experiment for calculation purposes.

MS was performed by Q Exactive plus mass spectrometer (TFS) for α-HIS IP and the PI-PLC experiment, Orbitrap XL (TFS) for α-FLAG IP initial screen, and Q Exactive HF mass spectrometer (TFS) for all other α-FLAG IPs.

Results were analyzed using the discoverer software version 1.4 for α-HIS IP, the MaxQuant software 1.5.2.8 (Cox et al., 2014) for α-FLAG IP initial screen and the PI-PLC experiment, and the MaxQuant software 2.1.1.0 (Cox et al., 2014) for all other α-FLAG IPs. The statistical analysis shown in raw data files was done using Perseus 1.6.7.0 software (Mathias Mann's group; Tyanova et al., 2016).

HCMV infection experiments

MRC-5 fibroblasts (parental or CLPTM1L KO) were plated 72 h prior to infection in a 24-well plate at a concentration of 100K cells/well. For uninfected control wells, the cells were plated at a concentration of 70K cells/well to achieve subconfluency by the time we harvested the infected cells. Infection was carried out with specified HCMV strains at an MOI of 1–2, and was enhanced by centrifugation at 800 *g* for 30 min. 24 hpi, we validated that both strains infected the cells at similar levels using intracellular FCM staining with α-CMV Ab (cat. MAB810X; Merck Millipore). Cells were harvested at 72 hpi to be used in WB or FCM experiments or at 24hpi for qPCR.

qPCR

Total RNA was isolated by the Quick-RNA Miniprep kit (cat. R1055; Zymo research) or the Total RNA mini-kit (cat. RBD050; Geneaid) according to the manufacturer's instructions. Total RNA was reverse transcribed with mMLV Reverse Transcriptase (cat. 28025013; Invitrogen) or Lunascript RT supermix kit (cat. E3010; New England Biolabs), according to the manufacturer's instructions. qPCR was used to measure mRNA expression as follows: cDNA was mixed with 150 µM of both the forward and reverse primers in a final volume of 5 µl and mixed with 5 µl of PowerTrack SUBR green master mix (cat. A46109; TFS). hUBC and hHPRT were used as endogenous reference genes for PCR quantification. PCR was performed on CFX connect Real-Time system (Bio-Rad).

The following primers were used (listed from 5′ to 3′):

hHPRT: Fw: 5′-TGACACTGGCAAAACAATGCA-3′, Rev: 5′-GGTCCTTTTCACCAGCAAGCT-3′. hUBC: Fw: 5′-ATTTGGGTC GCGGTTCTTG-3′, Rev: 5′-TGCCTTGACATTCTCGATGGT-3′.

US9: Fw: 5′-AACGCCCTCAGACTTGGAAC-3′, Rev: 5′-CTA CCTGGACACCGAAGCTG-3′.

PI-PLC experiment

Cells were plated in eight 10-cm plates each, 3 million cells/plate. Four plates of each cell type were designated for PI-PLC cleavage and the other four for MT control. The following day, cells were harvested with EDTA and DMEM without supplements (DMEM–) and collected to separate 50 ml tubes according to designation. The cells were then washed twice with DMEM to avoid FBS contamination and were transferred to 1.5 ml tubes and centrifuged to keep only the cell pellet. In the two PI-PLC tubes, cell pellets were resuspended with 25 units of PI-PLC (cat. P5542-25UN; Sigma-Aldrich) in 200 µl of the buffer, recommended by the manufacturer. In the MT tubes, pellets were resuspended with buffer only. After 4 h incubation at 37°C, the tubes were centrifuged and supernatants were collected. 50 µl of each tube was used for WB and the rest for MS analysis (as described above).

Label-free quantitation normalization was done with the assumption that most of the proteins did not change in abundance. Additional normalization to vinculin was performed as a measure of intracellular protein release due to cell death. For each normalization, the following ratios were calculated: (A) parental-PI-PLC/parental-MT and (B) parental-PI-PLC/KO-PI-PLC. The proteins were identified as potentially CLPTM1L-dependent if they answered the following selection criteria: (1) ratio A ≥ 1.5 in both normalization methods, (2) ratio B ≥ 2 in both normalization methods, and (3) the protein is known to be expressed on the cell membrane of human cells.

IF

Cells were grown on glass slides, then fixed and permeabilized by a 15-min incubation in RT with 4% PFA. Cells were blocked for 1 h at RT in CAS-block (cat. 008120; TFS) and then incubated overnight at 4°C with primary Abs diluted 1:50–200 in CAS-block. The next day, cells were washed and incubated for 1 h at RT in secondary Abs diluted 1:500 in PBS containing 5% BSA. Cells were then washed, treated for 5 min with DAPI, and covered with coverslips using mounting media (cat. P36980; TFS). Images were obtained with Olympus FV1000 confocal system with an inverted IX71 microscope, UPlanSApo 60X oil objective lens, and spectral-type fluorescence detector with Standard 3 confocal Channels. Images were processed using Olympus Fluoview FV1000 software.

Schematic diagrams

All schematic diagrams were created with BioRender.com.

Statistical analysis

We used Prism software version 9.5.1 (GraphPad) for statistical analysis. Specific statistical tests are mentioned throughout the

manuscript. Generally, we used two-tailed *t* test or one-way ANOVA, as indicated in figure legends. A statistical test was considered significant if $P < 0.05$. Gaussian distribution of data was assumed, but this was not formally tested.

Online supplemental material

Table S1 shows the summary of MS results of a Co-IP experiment, which was performed in various cell lines expressing the indicated constructs (all containing an N-terminal HIS tag) with α-HIS Ab or isotype control. Table S2 shows the summary of MS results of a Co-IP experiment, which was performed in two cell types using α-FLAG Ab. Table S3 shows a Co-IP experiment that was performed in two cell types using α-FLAG Ab. Data S1 shows MS results of α-HIS Co-IP (summarized in Table S1). Data S2 shows MS results of PI-PLC experiment. Data S3 shows MS results of α-FLAG Co-IP; PIG-T precipitates with CLPTM1L (summarized in Table S2). Data S4 shows MS results of α-FLAG Co-IP, SDS-PAGE; PIG-T detected at ∼65 kD (summarized in Table S3). Data S5 shows MS results of α-FLAG Co-IP; US9 interferes with CLPTM1L–PIG-T association (summarized in Fig. 7 G).

Acknowledgments

The authors would like to thank the Smoler Proteomics Center at the Technion Institute of Technology for MS analysis services. I. Kol is partially supported by the Foulkes Foundation fellowship.

This work was supported by the following grants awarded to O. Mandelboim: the Israel Innovation Authority Kamin grant 62615, the German-Israeli Foundation for Scientific Research and Development grant 1412-414.13/2017, the Israel Cancer Research Fund professorship grant, the Israel Science Foundation Israel-China grant 2554/18, the Ministry of Science and Technology-German Cancer Research Center grant 3-14931, and the Ministry of Science and Technology grant 3-14764.

Author contributions: E. Seidel generated preliminary results. I. Kol designed and performed experiments, analyzed results, and wrote the paper. A. Rishiq generated reagents and performed experiments. M. Cohen helped with HCMV propagation and associated experiments. S. Kahlon performed experiments. O. Pick and L. Dassa helped with reagent generation. N. Stein helped with reagent generation and edited the manuscript. Y. Bar-On, D.G. Wolf, E. Seidel, and O. Mandelboim supervised.

Disclosures: N. Stein reported personal fees from Immunai outside the submitted work. No other disclosures were reported.

Submitted: 21 July 2022
Revised: 3 April 2023
Accepted: 19 May 2023

References

Amsler, L., M. Verweij, and V.R. DeFilippis. 2013. The tiers and dimensions of evasion of the type I interferon response by human cytomegalovirus. *J. Mol. Biol.* 425:4857–4871. https://doi.org/10.1016/j.jmb.2013.08.023

Ashiru, O., P. Boutet, L. Fernández-Messina, S. Agüera-González, J.N. Skepper, M. Valés-Gómez, and H.T. Reyburn. 2010. Natural killer cell cytotoxicity is suppressed by exposure to the human NKG2D ligand MICA*008 that is shed by tumor cells in exosomes. *Cancer Res.* 70: 481–489. https://doi.org/10.1158/0008-5472.CAN-09-1688

Ashiru, O., S. López-Cobo, L. Fernández-Messina, S. Pontes-Quero, R. Pandolfi, H.T. Reyburn, and M. Valés-Gómez. 2013. A GPI anchor explains the unique biological features of the common NKG2D-ligand allele MICA*008. *Biochem. J.* 454:295–302. https://doi.org/10.1042/BJ20130194

Bauman, Y., N. Drayman, O. Ben-Nun-Shaul, A. Vitenstein, R. Yamin, Y. Ophir, A. Oppenheim, and O. Mandelboim. 2016. Downregulation of the stress-induced ligand ULBP1 following SV40 infection confers viral evasion from NK cell cytotoxicity. *Oncotarget*. 7:15369–15381. https://doi.org/10.18632/oncotarget.8085

Cox, J., M.Y. Hein, C.A. Luber, I. Paron, N. Nagaraj, and M. Mann. 2014. Accurate proteome-wide label-free quantification by delayed normalization and maximal peptide ratio extraction, termed MaxLFQ. *Mol. Cell. Proteomics*. 13:2513–2526. https://doi.org/10.1074/mcp.M113.031591

Diab, M., D. Schmiedel, E. Seidel, E. Bacharach, and O. Mandelboim. 2020. Human metapneumovirus escapes NK cell recognition through the downregulation of stress-induced ligands for NKG2D. *Viruses*. 12:781. https://doi.org/10.3390/v12070781

Eisenhaber, B., S. Maurer-Stroh, M. Novatchkova, G. Schneider, and F. Eisenhaber. 2003. Enzymes and auxiliary factors for GPI lipid anchor biosynthesis and post-translational transfer to proteins. *BioEssays*. 25: 367–385. https://doi.org/10.1002/bies.10254

Fernández-Messina, L., O. Ashiru, S. Agüera-González, H.T. Reyburn, and M. Valés-Gómez. 2011. The human NKG2D ligand ULBP2 can be expressed at the cell surface with or without a GPI anchor and both forms can activate NK cells. *J. Cell Sci.* 124:321–327. https://doi.org/10.1242/jcs.076042

Fernández-Messina, L., H.T. Reyburn, and M. Valés-Gómez. 2012. Human NKG2D-ligands: Cell biology strategies to ensure immune recognition. *Front. Immunol.* 3:299. https://doi.org/10.3389/fimmu.2012.00299

Fernández-Messina, L., H.T. Reyburn, and M. Valés-Gómez. 2016. A short half-life of ULBP1 at the cell surface due to internalization and proteosomal degradation. *Immunol. Cell Biol.* 94:479–485. https://doi.org/10.1038/icb.2016.2

Galian, C., P. Björkholm, N. Bulleid, and G. von Heijne. 2012. Efficient glycosylphosphatidylinositol (GPI) modification of membrane proteins requires a C-terminal anchoring signal of marginal hydrophobicity. *J. Biol. Chem.* 287:16399–16409. https://doi.org/10.1074/jbc.M112.350009

Gennarini, G., A. Bizzoca, S. Picocci, D. Puzzo, P. Corsi, and A.J.W. Furley. 2017. The role of Gpi-anchored axonal glycoproteins in neural development and neurological disorders. *Mol. Cell. Neurosci.* 81:49–63. https://doi.org/10.1016/j.mcn.2016.11.006

Georgopoulou, U., A. Dimitriadis, P. Foka, E. Karamichali, and A. Mamalaki. 2014. Hepcidin and the iron enigma in HCV infection. *Virulence*. 5: 465–476. https://doi.org/10.4161/viru.28508

Gerber, L.D., K. Kodukula, and S. Udenfriend. 1992. Phosphatidylinositol glycan (PI-G) anchored membrane proteins. Amino acid requirements adjacent to the site of cleavage and PI-G attachment in the COOH-terminal signal peptide. *J. Biol. Chem.* 267:12168–12173. https://doi.org/10.1016/S0021-9258(19)49819-0

Gíslason, M.H., H. Nielsen, J.J. Almagro Armenteros, and A.R. Johansen. 2021. Prediction of GPI-anchored proteins with pointer neural networks. *Curr. Res. Biotechnol.* 3:6–13. https://doi.org/10.1016/j.crbiot.2021.01.001

Halenius, A., C. Gerke, and H. Hengel. 2015. Classical and non-classical MHC I molecule manipulation by human cytomegalovirus: So many targets—but how many arrows in the quiver? *Cell. Mol. Immunol.* 12:139–153. https://doi.org/10.1038/cmi.2014.105

Hein, Z., N.M. Hooper, and H.Y. Naim. 2009. Association of a GPI-anchored protein with detergent-resistant membranes facilitates its trafficking through the early secretory pathway. *Exp. Cell Res.* 315:348–356. https://doi.org/10.1016/j.yexcr.2008.10.038

Hussein, N.H., N.S. Amin, and H.M. El Tayebi. 2020. GPI-AP: Unraveling a new class of Malignancy mediators and potential immunotherapy targets. *Front. Oncol.* 10:537311. https://doi.org/10.3389/fonc.2020.537311

Jackson, S.E., G.M. Mason, and M.R. Wills. 2011. Human cytomegalovirus immunity and immune evasion. *Virus Res.* 157:151–160. https://doi.org/10.1016/j.virusres.2010.10.031

James, M.A., H.G. Vikis, E. Tate, A.L. Rymaszewski, and M. You. 2014. CRR9/CLPTM1L regulates cell survival signaling and is required for Ras transformation and lung tumorigenesis. *Cancer Res.* 74:1116–1127. https://doi.org/10.1158/0008-5472.CAN-13-1617

James, M.A., W. Wen, Y. Wang, L.A. Byers, J.V. Heymach, K.R. Coombes, L. Girard, J. Minna, and M. You. 2012. Functional characterization of

CLPTM1L as a lung cancer risk candidate gene in the 5p15.33 locus. *PLoS One*. 7:e36116. https://doi.org/10.1371/journal.pone.0036116

Kennard, M.L., D.R. Richardson, R. Gabathuler, P. Ponka, and W.A. Jefferies. 1995. A novel iron uptake mechanism mediated by GPI-anchored human p97. *EMBO J.* 14:4178–4186. https://doi.org/10.1002/j.1460-2075.1995.tb00091.x

Kinoshita, T. 2020. Biosynthesis and biology of mammalian GPI-anchored proteins. *Open Biol.* 10:190290. https://doi.org/10.1098/rsob.190290

Kinoshita, T., and M. Fujita. 2016. Biosynthesis of GPI-anchored proteins: Special emphasis on GPI lipid remodeling. *J. Lipid Res.* 57:6–24. https://doi.org/10.1194/jlr.R063313

Klussmeier, A., C. Massalski, K. Putke, G. Schäfer, J. Sauter, D. Schefzyk, J. Pruschke, J. Hofmann, D. Fürst, R. Carapito, et al. 2020. High-throughput MICA/B Genotyping of over two Million samples: Workflow and allele frequencies. *Front. Immunol.* 11:314. https://doi.org/10.3389/fimmu.2020.00314

Manea, E. 2018. A step closer in defining glycosylphosphatidylinositol anchored proteins role in health and glycosylation disorders. *Mol. Genet. Metab. Rep.* 16:67–75. https://doi.org/10.1016/j.ymgmr.2018.07.006

Martin, M., P. Sandhu, R. Kumar, and N.J. Buchkovich. 2022. The immune-specific E3 ubiquitin ligase MARCH1 is upregulated during human cytomegalovirus infection to regulate iron levels. *J. Virol.* 96:e0180621. https://doi.org/10.1128/jvi.01806-21

McSharry, B.P., H.-G. Burgert, D.P. Owen, R.J. Stanton, V. Prod'homme, M. Sester, K. Koebernick, V. Groh, T. Spies, S. Cox, et al. 2008. Adenovirus E3/19K promotes evasion of NK cell recognition by intracellular sequestration of the NKG2D ligands major histocompatibility complex class I chain-related proteins A and B. *J. Virol.* 82:4585–4594. https://doi.org/10.1128/JVI.02251-07

Muckenthaler, M.U., S. Rivella, M.W. Hentze, and B. Galy. 2017. A red carpet for iron metabolism. *Cell*. 168:344–361. https://doi.org/10.1016/j.cell.2016.12.034

Nachmani, D., N. Stern-Ginossar, R. Sarid, and O. Mandelboim. 2009. Diverse herpesvirus microRNAs target the stress-induced immune ligand MICB to escape recognition by natural killer cells. *Cell Host Microbe*. 5:376–385. https://doi.org/10.1016/j.chom.2009.03.003

Ni, Z., Q. Chen, Y. Lai, Z. Wang, L. Sun, X. Luo, and X. Wang. 2016. Prognostic significance of CLPTM1L expression and its effects on migration and invasion of human lung cancer cells. *Cancer Biomark.* 16:445–452. https://doi.org/10.3233/CBM-160583

Ni, Z., K. Tao, G. Chen, Q. Chen, J. Tang, X. Luo, P. Yin, J. Tang, and X. Wang. 2012. CLPTM1L is overexpressed in lung cancer and associated with apoptosis. *PLoS One*. 7:e52598. https://doi.org/10.1371/journal.pone.0052598

Nobre, L.V., K. Nightingale, B.J. Ravenhill, R. Antrobus, L. Soday, J. Nichols, J.A. Davies, S. Seirafian, E.C.Y. Wang, A.J. Davison, et al. 2019. Human cytomegalovirus interactome analysis identifies degradation hubs, domain associations and viral protein functions. *Elife*. 8:e49894. https://doi.org/10.7554/eLife.49894

Ohishi, K., K. Nagamune, Y. Maeda, and T. Kinoshita. 2003. Two subunits of glycosylphosphatidylinositol transamidase, GPI8 and PIG-T, form a functionally important intermolecular disulfide bridge. *J. Biol. Chem.* 278:13959–13967. https://doi.org/10.1074/jbc.M300586200

Park, A., E.A. Ra, T.A. Lee, H.J. Choi, E. Lee, S. Kang, J.Y. Seo, S. Lee, and B. Park. 2019. HCMV-encoded US7 and US8 act as antagonists of innate immunity by distinctively targeting TLR-signaling pathways. *Nat. Commun.* 10:4670. https://doi.org/10.1038/s41467-019-12641-4

De Pelsmaeker, S., N. Romero, M. Vitale, and H.W. Favoreel. 2018. Herpesvirus evasion of natural killer cells. *J. Virol.* 92:e02105-17. https://doi.org/10.1128/jvi.02105-17

Pierleoni, A., P.L. Martelli, and R. Casadio. 2008. PredGPI: A GPI-anchor predictor. *BMC Bioinformatics*. 9:392. https://doi.org/10.1186/1471-2105-9-392

Raulet, D.H., S. Gasser, B.G. Gowen, W. Deng, and H. Jung. 2013. Regulation of ligands for the NKG2D activating receptor. *Annu. Rev. Immunol.* 31:413–441. https://doi.org/10.1146/annurev-immunol-032712-095951

Risti, M., and M.D. Bicalho. 2017. MICA and NKG2D: Is there an Impact on kidney transplant outcome? *Front. Immunol.* 8:179. https://doi.org/10.3389/fimmu.2017.00179

Robinson, J., D.J. Barker, X. Georgiou, M.A. Cooper, P. Flicek, and S.G.E. Marsh. 2020. IPD-IMGT/HLA database. *Nucleic Acids Res.* 48:D948–D955. https://doi.org/10.1093/nar/gkz950

Schmiedel, D., and O. Mandelboim. 2018. NKG2D ligands-critical targets for cancer immune escape and therapy. *Front. Immunol.* 9:2040. https://doi.org/10.3389/fimmu.2018.02040

Seidel, E., L. Dassa, S. Kahlon, B. Tirosh, A. Halenius, T. Seidel Malkinson, and O. Mandelboim. 2021a. A slowly cleaved viral signal peptide acts as a protein-integral immune evasion domain. *Nat. Commun.* 12:2061. https://doi.org/10.1038/s41467-021-21983-x

Seidel, E., L. Dassa, C. Schuler, E. Oiknine-Djian, D.G. Wolf, V.T.K. Le-Trilling, and O. Mandelboim. 2021b. The human cytomegalovirus protein UL147A downregulates the most prevalent MICA allele: MICA*008, to evade NK cell-mediated killing. *PLoS Pathog.* 17:e1008807. https://doi.org/10.1371/journal.ppat.1008807

Seidel, E., V.T.K. Le, Y. Bar-On, P. Tsukerman, J. Enk, R. Yamin, N. Stein, D. Schmiedel, E. Oiknine Djian, Y. Weisblum, et al. 2015. Dynamic Co-evolution of host and pathogen: HCMV downregulates the prevalent allele MICA-008 to escape elimination by NK cells. *Cell Rep.* 10:968–982. https://doi.org/10.1016/j.celrep.2015.01.029

Shalem, O., N.E. Sanjana, E. Hartenian, X. Shi, D.A. Scott, T. Mikkelson, D. Heckl, B.L. Ebert, D.E. Root, J.G. Doench, and F. Zhang. 2014. Genome-scale CRISPR-Cas9 knockout screening in human cells. *Science*. 343:84–87. https://doi.org/10.1126/science.1247005

Stern-Ginossar, N., N. Elefant, A. Zimmermann, D.G. Wolf, N. Saleh, M. Biton, E. Horwitz, Z. Prokocimer, M. Prichard, G. Hahn, et al. 2007. Host immune system gene targeting by a viral miRNA. *Science*. 317:376–381. https://doi.org/10.1126/science.1140956

Suemizu, H., M. Radosavljevic, M. Kimura, S. Sadahiro, S. Yoshimura, S. Bahram, and H. Inoko. 2002. A basolateral sorting motif in the MICA cytoplasmic tail. *Proc. Natl. Acad. Sci. USA*. 99:2971–2976. https://doi.org/10.1073/pnas.052701099

Sun, Y., Q. Bao, B. Xuan, W. Xu, D. Pan, Q. Li, and Z. Qian. 2018. Human cytomegalovirus protein pUL38 prevents premature cell death by binding to ubiquitin-specific protease 24 and regulating iron metabolism. *J. Virol.* 92:e00191-18. https://doi.org/10.1128/jvi.00191-18

Takida, S., Y. Maeda, and T. Kinoshita. 2008. Mammalian GPI-anchored proteins require p24 proteins for their efficient transport from the ER to the plasma membrane. *Biochem. J.* 409:555–562. https://doi.org/10.1042/BJ20070234

Tyanova, S., T. Temu, P. Sinitcyn, A. Carlson, M.Y. Hein, T. Geiger, M. Mann, and J. Cox. 2016. The Perseus computational platform for comprehensive analysis of (prote)omics data. *Nat. Methods*. 13:731–740. https://doi.org/10.1038/nmeth.3901

Vahdati-Ben Arieh, S., N. Laham, C. Schechter, J.W. Yewdell, J.E. Coligan, and R. Ehrlich. 2003. A single viral protein HCMV US2 affects antigen presentation and intracellular iron homeostasis by degradation of classical HLA class I and HFE molecules. *Blood*. 101:2858–2864. https://doi.org/10.1182/blood-2002-07-2158

Wang, Y., A.K. Menon, Y. Maki, Y.S. Liu, Y. Iwasaki, M. Fujita, P.A. Guerrero, D.V. Silva, P.H. Seeberger, Y. Murakami, and T. Kinoshita. 2022. Genome-wide CRISPR screen reveals CLPTM1L as a lipid scramblase required for efficient glycosylphosphatidylinositol biosynthesis. *Proc. Natl. Acad. Sci. USA*. 119:e2115083119. https://doi.org/10.1073/pnas.2115083119

Weekes, M.P., P. Tomasec, E.L. Huttlin, C.A. Fielding, D. Nusinow, R.J. Stanton, E.C.Y. Wang, R. Aicheler, I. Murrell, G.W.G. Wilkinson, et al. 2014. Quantitative temporal viromics: An approach to investigate host-pathogen interaction. *Cell*. 157:1460–1472. https://doi.org/10.1016/j.cell.2014.04.028

Wilkinson, G.W.G., P. Tomasec, R.J. Stanton, M. Armstrong, V. Prod'homme, R. Aicheler, B.P. McSharry, C.R. Rickards, D. Cochrane, S. Llewellyn-Lacey, et al. 2008. Modulation of natural killer cells by human cytomegalovirus. *J. Clin. Virol.* 41:206–212. https://doi.org/10.1016/j.jcv.2007.10.027

Yamamoto, K., A. Okamoto, S. Isonishi, K. Ochiai, and Y. Ohtake. 2001. A novel gene, CRR9, which was up-regulated in CDDP-resistant ovarian tumor cell line, was associated with apoptosis. *Biochem. Biophys. Res. Commun.* 280:1148–1154. https://doi.org/10.1006/bbrc.2001.4250

Yang, L., H. Wang, X. Yang, Q. Wu, P. An, X. Jin, W. Liu, X. Huang, Y. Li, S. Yan, et al. 2020. Auranofin mitigates systemic iron overload and induces ferroptosis via distinct mechanisms. *Signal Transduct. Target. Ther.* 5:138. https://doi.org/10.1038/s41392-020-00253-0

Zhang, H., J. Su, B. Li, Y. Gao, M. Liu, L. He, H. Xu, Y. Dong, X.C. Zhang, and Y. Zhao. 2022. Structure of human glycosylphosphatidylinositol transamidase. *Nat. Struct. Mol. Biol.* 29:203–209. https://doi.org/10.1038/s41594-022-00726-6

Zhang, Y., A.M. Lazaro, B. Lavingia, and P. Stastny. 2001. Typing for all known MICA alleles by group-specific PCR and SSOP. *Hum. Immunol.* 62:620–631. https://doi.org/10.1016/S0198-8859(01)00241-5

Supplemental material

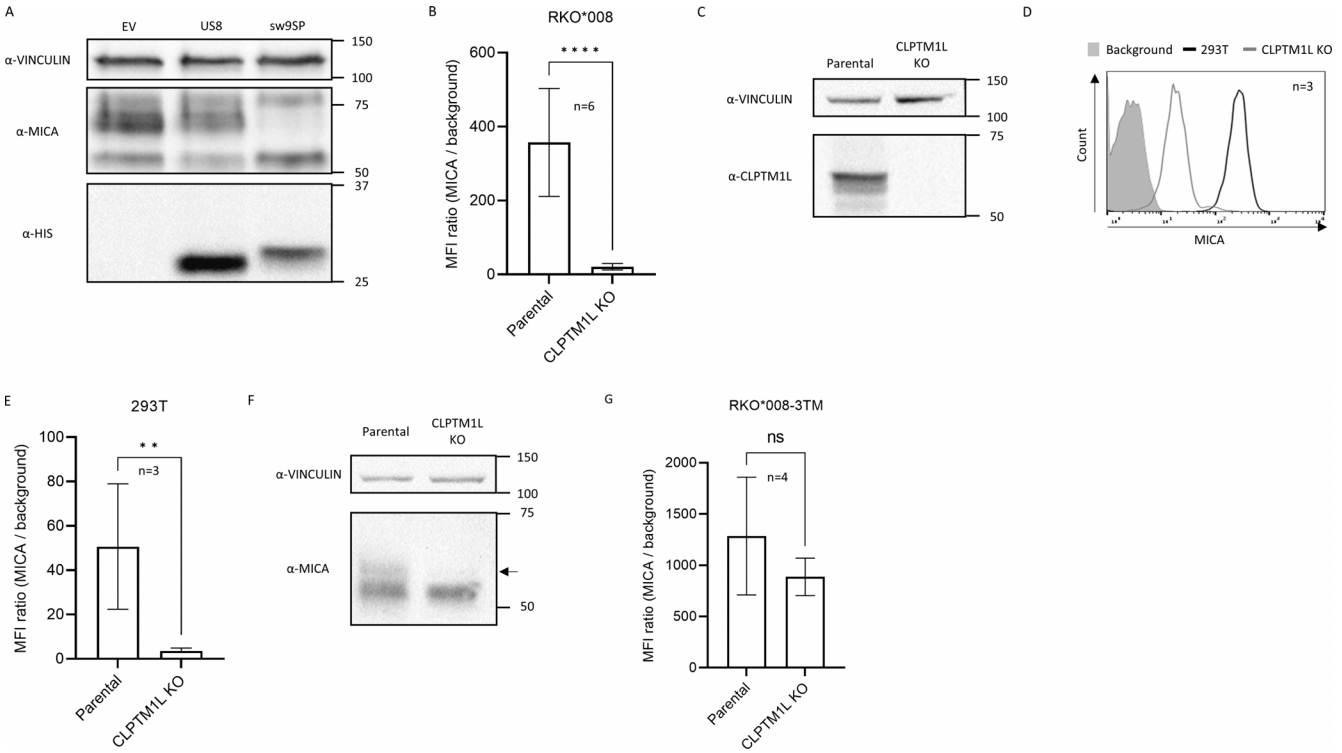

Figure S1. **MICA*008's maturation and surface expression is downregulated upon CLPTM1L KO. (A)** RKO*008 cells, co-expressing one of the following: EV, US8-HIS (US8), and sw9SP-HIS (sw9SP), were lysed and analyzed by WB. Detection Abs are indicated next to each blot. **(B)** Median fluorescence intensity (MFI) quantification of MICA*008 in RKO*008 CLPTM1L KO cells. RKO*008 cells, either parental or CLPTM1L KO, were analyzed by FCM with α-MICA Ab (staining shown in Fig. 3 B). In each cell line, the α-MICA MFI was divided by the background (secondary Ab only). Figure shows mean and SEM for six independent experiments. ****P < 0.0001; ratio paired, two-tailed *t* test. **(C)** Parental and CLPTM1L KO 293T cells were lysed and analyzed by WB. Detection Abs are indicated on the left. **(D)** Cells as in C were stained with α-MICA Ab and analyzed by FCM. 293T, black line, CLPTM1L KO, gray line, background (secondary Ab only), gray-filled histogram. **(E)** MFI quantification of MICA*008 in 293T CLPTM1L KO cells. Cells as in C were used, and MFI was quantified as in B. Data shows mean and SEM for three independent experiments. **P < 0.01; ratio paired, two-tailed *t* test. **(F)** Cells as in C were lysed and analyzed by WB. Detection Abs are indicated on the left. Arrow indicates the post-ER form of MICA*008. **(G)** MFI quantification of MICA*008-ULBP3TM upon CLPTM1L KO. RKO cells expressing the MICA*008-ULBP3TM mutant (RKO*008-3TM), either parental or CLPTM1L KO, were analyzed by FCM with α-MICA Ab (staining shown in Fig. 3 K). In each cell line, the α-MICA MFI was divided by the background (secondary Ab only). Figure shows mean and SEM for four independent experiments. ns, non-significant; ratio paired, two-tailed *t* test. Source data are available for this figure: SourceData FS1.

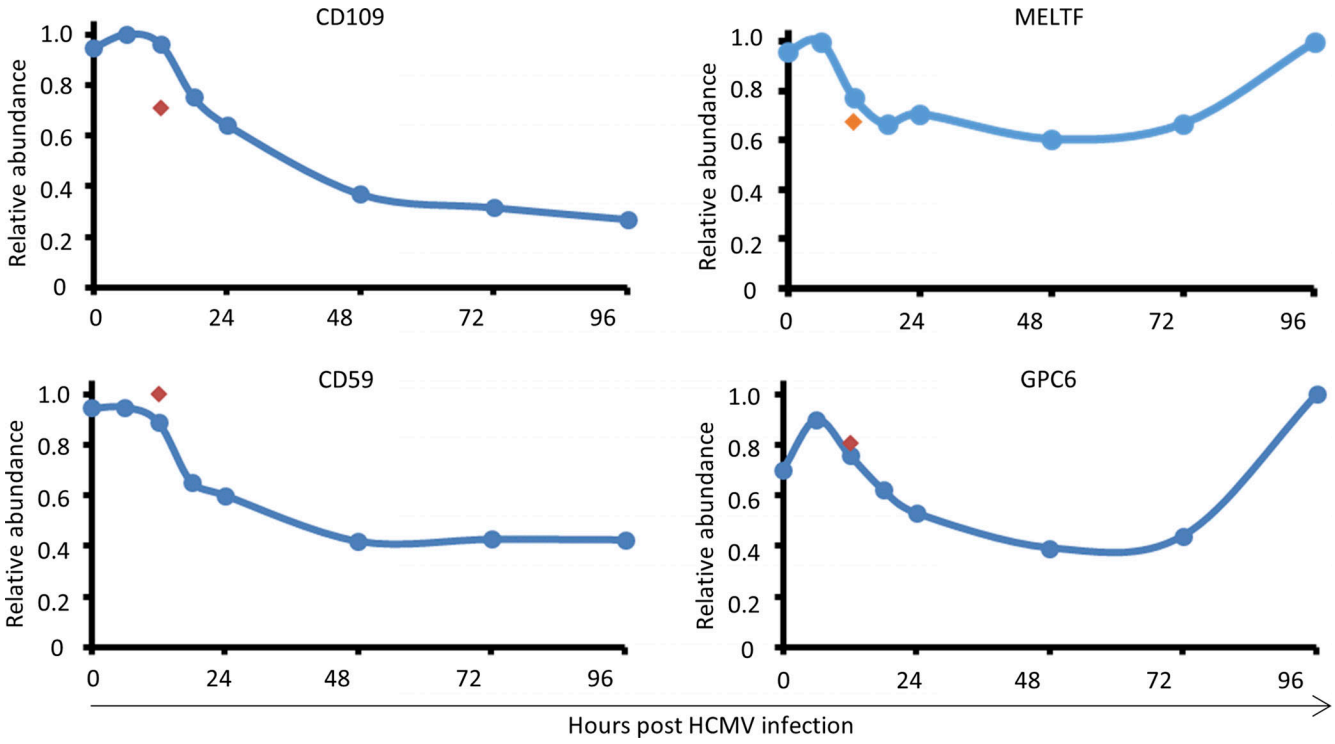

Figure S2. **Surface levels of CD109, CD59, MELTF, and GPC6 at different time points during HCMV infection of human foreskin fibroblasts.** Data was generated using previously published surface and total cell proteomics data by Weekes et al. (2014). Red diamond, 12 h after incubation with UV-inactivated virus.

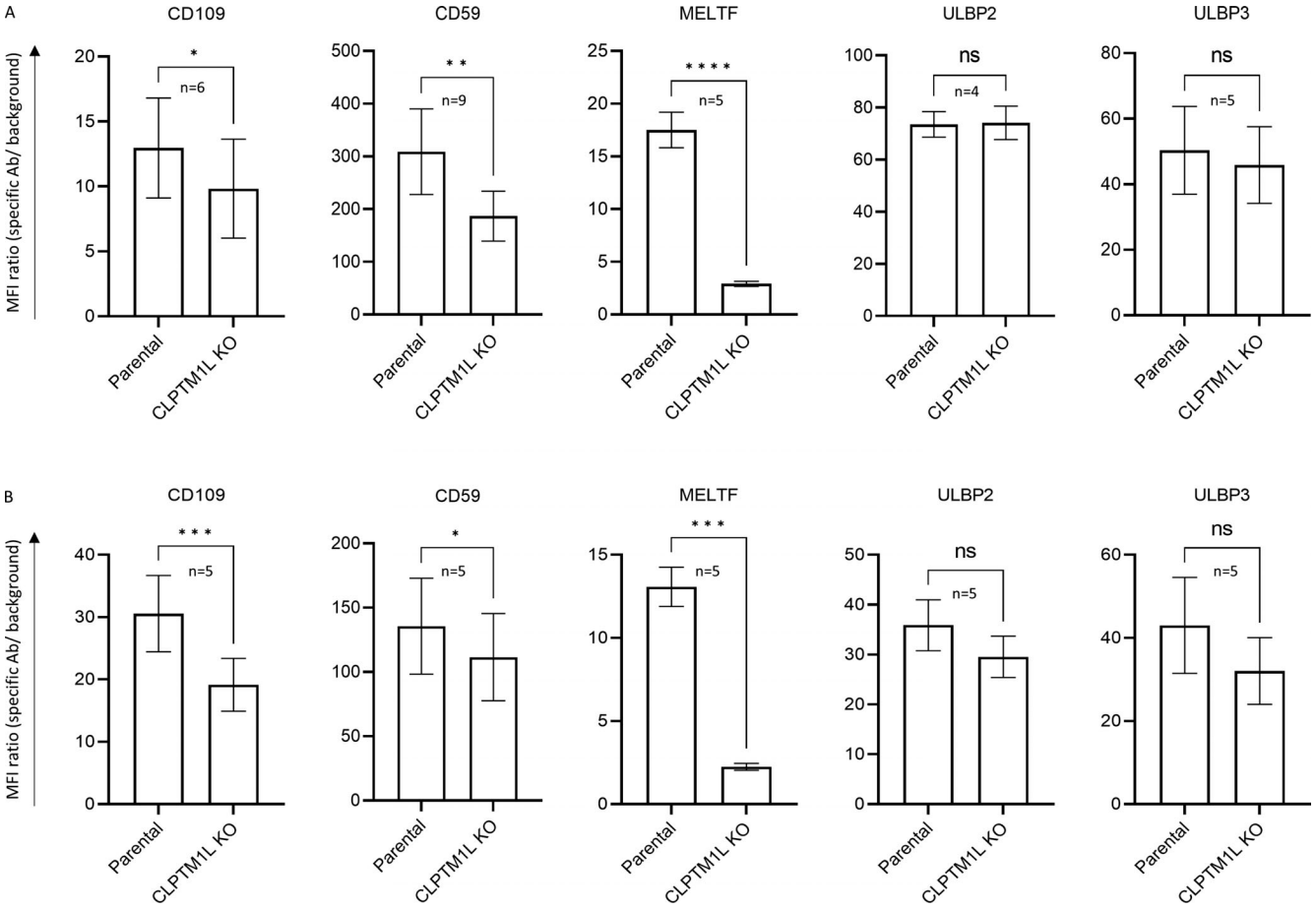

Figure S3. **Three GPI-anchored proteins (CD109, CD59, and MELTF) depend on CLPTM1L for their surface expression. (A)** RKO*008 cells, either parental or CLPTM1L KO, were analyzed by FCM with the indicated Abs (staining shown in Fig. 5 C). Specific antibody MFIs were divided by backgrounds (secondary antibody only or PE-conjugated isotype control). Data show mean and SEM for at least three independent experiments per antibody. *P < 0.05; **P < 0.01; ****P < 0.0001; ns, non-significant; ratio paired, two-tailed *t* test. **(B)** 293T cells, either parental or CLPTM1L KO, were analyzed by flFCM with the indicated antibodies (staining shown in Fig. 5 D). MFI was then quantified as in A. Figure shows mean and SEM for three independent experiments per Ab. *, P < 0.05; ***, P < 0.001; ns, non-significant; ratio paired, two-tailed *t* test.

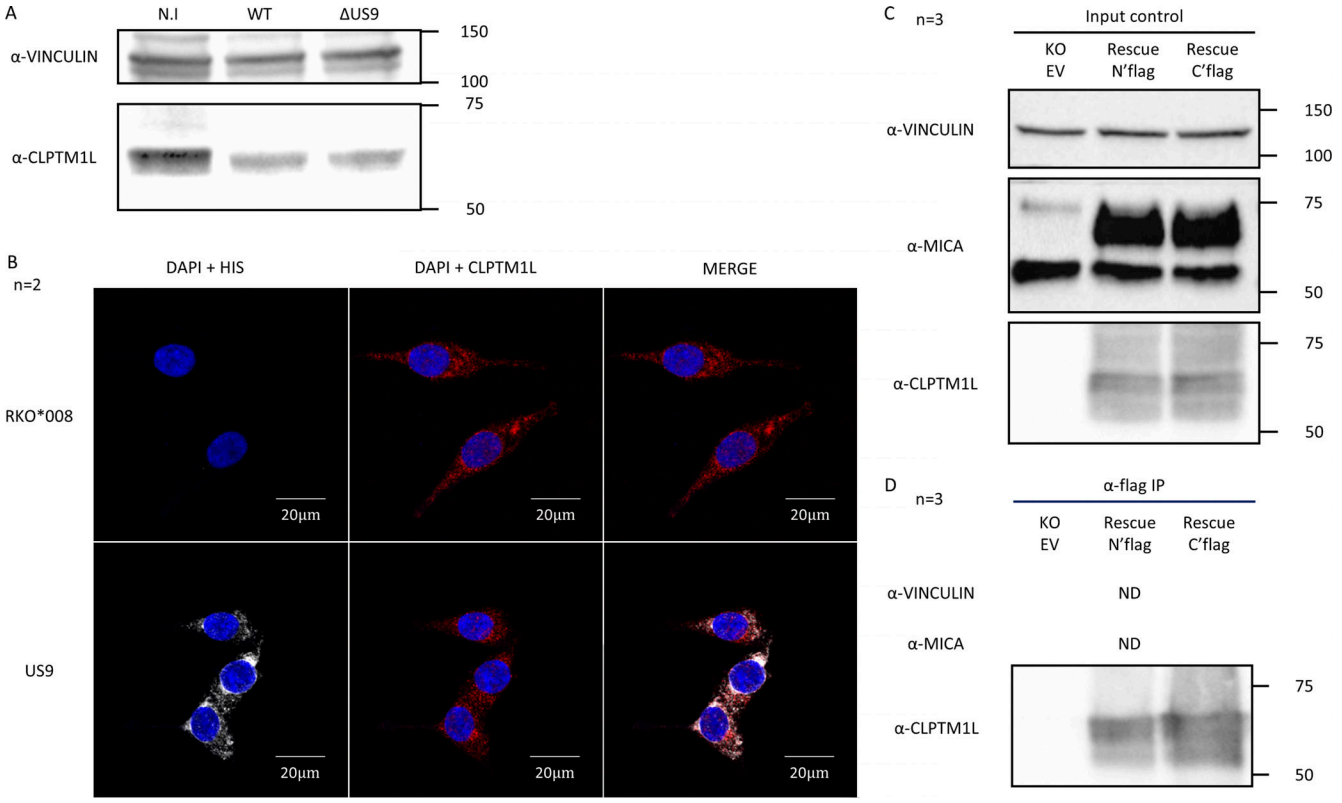

Figure S4. **US9 does not act by affecting CLPTM1L protein levels, cellular localization, or interaction with MICA*008. (A)** MRC-5 fibroblasts were infected with AD169varL (WT) or its previously generated US9 deletion mutant, ΔUS9. Uninfected cells were used as control (N.I). At 72 hpi the cells were lysed and analyzed by WB. Detection Abs are indicated on the left. **(B)** Intracellular localization of CLPTM1L and US9 demonstrated by confocal microscopy. RKO*008 cells, either parental (RKO*008) or co-expressing US9-HIS (US9), were stained with an α-HIS tag Ab (white) and an α-CLPTM1L Ab (red). Nuclei were stained with DAPI (blue). Representative of two independent experiments. **(C and D)** Co-IP performed in RKO*008 CLPTM1L KO cells expressing an EV (KO EV), an N'FLAG tagged CLPTM1L (Rescue N'FLAG), or a C'FLAG tagged CLPTM1L (Rescue C'FLAG). Detection Abs are indicated next to each blot; ND, not detected. **(C)** Cell lysates before precipitation were used as input control. **(D)** Precipitation Ab used was α-FLAG. Source data are available for this figure: SourceData FS4.

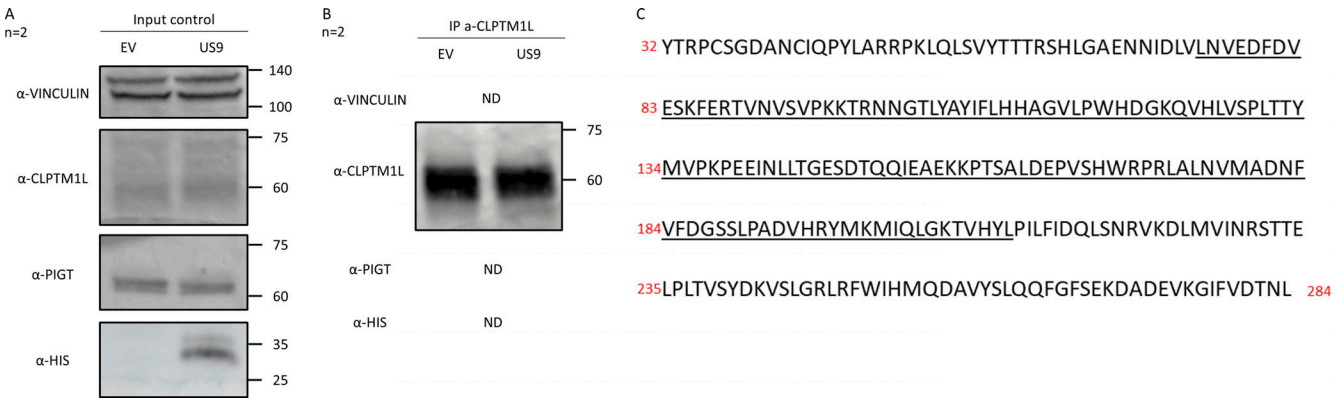

Figure S5. **Both US9 and PIG-T bind the same region in CLPTM1L. (A and B)** Co-IP performed in RKO*008 cells expressing an EV or US9-HIS (US9). Detection Abs are indicated next to each blot; ND, not detected. **(A)** Cell lysates before precipitation were used as input control. **(B)** Precipitation Ab used was α-CLPTM1L. **(C)** The amino acid sequence of CLPTM1L's first luminal domain. The α-CLPTM1L Ab used in B is directed against the underlined immunogen sequence. Amino acid numbers are shown in red.

Provided online are three tables and five datasets. Table S1 shows the summary of MS results of a Co-IP experiment, which was performed in various cell lines expressing the indicated constructs (all containing an N-terminal HIS tag) with anti-HIS antibody, or isotype control. Table S2 shows the summary of MS results of a Co-IP experiment, which was performed in two cell types using

anti-FLAG antibody. Table S3 shows a Co-IP experiment that was performed in two cell types using anti-FLAG antibody. Data S1 shows MS results of anti-HIS Co-IP (summarized in Table S1). Data S2 shows MS results of PI-PLC experiment. Data S3 shows MS results of anti-FLAG Co-IP; PIG-T precipitates with CLPTM1L (summarized in Table S2). Data S4 shows MS results of anti-FLAG Co-IP, SDS-PAGE; PIG-T detected at ∼65 kD (summarized in Table S3). Data S5 shows MS results of anti-FLAG Co-IP; US9 interferes with CLPTM1L–PIG-T association (summarized in Fig. 7 G).